

Validation of the Stand-up Technique for Total Skin Irradiation by Monte Carlo

Simulation

by

Wen-Chih Tseng

Graduate Program in Medical Physics
Duke University

Date: _____

Approved:

Qiuwen Wu, Supervisor

Rathnayaka Gunasingha

Oana Craciunescu

Christopher Kelsey

Thesis submitted in partial fulfillment of
the requirements for the degree of
Master of Science in the
Medical Physics in the Graduate School
of Duke University

2019

ABSTRACT

Validation of the Stand-up Technique for Total Skin Irradiation by Monte Carlo

Simulation

by

Wen-Chih Tseng

Graduate Program in Medical Physics
Duke University

Date: _____

Approved:

Qiuwen Wu, Supervisor

Rathnayaka Gunasingha

Oana Craciunescu

Christopher Kelsey

An abstract of a thesis submitted in partial
fulfillment of the requirements for the degree
of Master of Science in the
Medical Physics in the Graduate School of
Duke University

2019

Copyright by
Wen-Chih Tseng
2019

Abstract

Purpose/Objective(s): The standard total skin irradiation (TSI) procedure for patients with Mycosis fungoides at our clinic is the Stanford technique where dual electron beams are directed toward patient standing at an extended source to skin distance (SSD) of 300 cm. Patients rotate along the cranial-caudal axis in 6 directions to get full coverage to skin surface. The purposes of this study are to validate the commissioning dosimetric data using Monte Carlo (MC) systems, and to investigate the effect of scattering filter on the standard stand-up technique with a single beam.

Materials/Methods: The first MC system is the EGSnrc environment with BEAMnrc and DOSXYZnrc packages, which has been the standard MC simulation system used in the radiation therapy field. In this study, extended SSD with electron beam was tested, which is not a common use of EGSnrc. The second system is the VirtuaLinac, a recently developed cloud-based application from Varian for research purpose based on GEANT4 platform. For both MC systems, the same phase space files which have been previously validated were used. At each direction, a dual-field electron beam with jaws opening of $36 \times 36 \text{ cm}^2$ and gantry angle at $\pm 19^\circ$ degrees from horizontal direction was used. The following quantities were studied and compared with the measurements during commissioning: for each field/direction at the treatment SSD, the percentage depth dose (PDD), the profiles at the depth of maximum, and the absolute dosimetric output on a flat solid water phantom; the composite dose distribution on a

cylindrical phantom of 30 cm diameter. For the investigation part, the materials (Cu, Fe, Au, Zn, Ag) were chosen because of their stability and availability. The thickness ranges from 0.05 mm to 0.55 mm, depending on characteristics of materials. The extended source to skin distance (SSD) from 250 cm to 350 cm were studied. For each material, we vary the thickness and SSD, to evaluate following quantities: percent depth dose (PDD), profiles and output at d_{\max} , and compared them with the standard dual beams at treatment SSD.

Results: For the dual-field electron beam from one direction, the average(maximum) difference in profiles between EGSnrc/VirtuaLinac and measurement were -5.5% (-8.7%) and 0.9% (2.0%). Both d_{\max} (1.1 cm) and R_{50} (2.1 cm) in PDD of both MC systems agreed well with the measurements within 1 mm. The X-ray contamination at 15 cm depth was 0.5%/0.6% for EGSnrc/ VirtuaLinac, compared with the measured value of 0.8%. The output was -2.4%/-3.2% difference for EGSnrc/VirtuaLinac when compared with measurement. When radiation from all six directions are combined on a cylindrical phantom, the ratio of output at the surface from 6 directions to a single direction, defined as B-factor, is 3.1 from both MC systems and the measurement. The d_{\max} also shifted toward the surface at 0.15 cm. The X-ray contamination of all fields was 1.2 % and 1.3% for EGSnrc and VirtuaLinac, compared with 2% in the measurements. For the investigation part, no material shows acceptable profile flatness ($\pm 10\%$ within the central 160 cm) at 250 cm SSD. At 300 cm SSD, Au (0.1

mm), Ag (0.25 mm), and Cu (0.45 mm) are acceptable. Zn (0.45 mm) requires 325 cm SSD to meet the requirement. For these 4 configurations, the d_{\max} is 0.87-0.99 cm, similar to dual beam (0.97 cm); R_{50} is 1.85-1.91 cm, compared with dual beam of 2.06 cm; the output ranges from 0.025-0.029, lower than the dual beam (0.080). The composite fields for 4 configurations, the d_{\max} is 0.1 cm, compared with dual beam (0.16 cm). The surface dose is 97%, similar to dual beam (96%). B-factor is 3.3-3.4, compared with dual beam (3.1). The maximum x-ray contamination is 3%, slightly higher than dual beam (2%).

Conclusions: The results from both Monte Carlo systems in general agree well with the measurement for the validation part. Furthermore, MC results suggest the stand-up TSI technique can be implemented using a single beam if the customized filter is used. In addition to those measurable quantities, the Monte Carlo simulation can provide further information such as the full dose distribution of the patient phantom, thus become the foundation for investigations for future technique optimizations.

Contents

Abstract	1
List of Tables.....	7
List of Figures	8
Acknowledgements.....	11
1. Introduction	12
1.1 Total Skin Irradiation.....	12
1.2 Total Skin Irradiation Technique	12
1.3 Monte Carlo Method	15
1.4 The Objectives of the study.....	16
2. Material and Methods	19
2.1 Commissioning Measurement at Duke Radiation Oncology	19
2.1.1 TSI Stand-up Technique.....	20
2.1.2 TSI Lay-down Technique.....	22
2.2 Monte Carlo Simulations	23
2.2.1 EGSnrc	23
2.2.1.1 Validate the dosimetric data at isocenter	25
2.2.1.2 Validate the dosimetric data at treatment distance for the Stand-up technique.....	26
2.2.1.3 Validate the dosimetric data at treatment distance for the Lay-down technique.....	26
2.2.1.4 Investigation of effect of filter design for the TSI Stand-up technique	27
2.2.2 VirtuaLinac.....	28

3. Results and Discussion	31
3.1 Validation of Monte Carlo Simulation at 100 cm SSD	31
3.2 Validation of Monte Carlo Simulation at 300 cm SSD for the Stand-up technique	36
3.2.1 Profiles for single-field electron beam (-19 degrees).....	36
3.2.2 Profiles for dual-field electron beam (± 19 degrees).....	38
3.2.3 Dose distribution on a cylindrical phantom for the stand-up technique	42
3.2.3.1 Composite PDD for single, three, and six dual-field electron beams on a cylindrical phantom	42
3.2.3.2 Composite PDD along 0, 30, and 60 degree for six dual-field electron beams on a cylindrical phantom	47
3.2.3.3 Off axis PDD (0, 40, 80 cm from the central slice) for six dual-field electron beams on a cylindrical phantom	49
3.2.3.4 Composite PDD for six dual-field electron beams on a cylindrical phantom with different sizes (20, 30, and 40 cm diameter).....	53
3.2.4 Output factor, Body factor, and X-ray contamination.....	55
3.3 Validation of Monte Carlo Simulation for the Lay-down technique.....	56
3.3.1 Profiles for Vertex fields.....	56
3.3.2 Profiles for Oblique fields	58
3.3.3 Composite dose distribution on a cylindrical phantom for the lay-down technique	59
3.3.4 Output factor, Body factor, and X-ray contamination.....	61
3.4 Investigation of effect of filter design for the stand-up technique.....	62
3.4.1 Profiles for single beam on a flat solid water phantom.....	62
3.4.2 Dose distribution for composite fields on a cylindrical phantom	66

4. Future Work	69
4.1 Investigation of the gantry rotation issue in EGSnrc	69
4.2 Implementation of a customized scattering filter within VirtuaLinac	70
4.3 Optimization for the current standard TSI stand-up technique.....	70
5. Conclusion	72
References	74

List of Tables

Table 1 : Dosimetric quantities of central axis PDD with 36x36 cm ² field size at isocenter	35
Table 2 : Dosimetric quantities of central axis PDD at treatment distance for single field electron beam	38
Table 3 : Dosimetric quantities of PDD at treatment distance for one dual-field electron beam.....	42
Table 4 : Dosimetric quantities of PDD at treatment distance for six dual-field electron beams.....	43
Table 5 : Dosimetric quantities for single, three, six dual-field electron beams at central slice of 30 cm diameter cylindrical phantom	46
Table 6 : Central slice PDDs along 0, 30, 60 degrees arrows shown in figure 16	49
Table 7 : Dosimetric quantities for different phantom sizes (20, 30, and 40 cm).....	55
Table 8: Dosimetric quantities for a single direction	65
Table 9: Dosimetric quantities for composite fields.....	67

List of Figures

Figure 1 : Side view (Left) and top view (Right) of the customized copper filter	14
Figure 2 : A general workflow of EGSnrc	27
Figure 3 : A general workflow of VirtuaLinac.....	30
Figure 4 : X profile (1 cm depth) of 36x36 cm ² field size at isocenter	33
Figure 5 : Y profile (1 cm depth) of 36x36 cm ² field size at isocenter	34
Figure 6 : Central axis PDD of 36x36 cm ² field size at isocenter	35
Figure 7 : X profile (1 cm depth) at treatment distance for single field electron beam	36
Figure 8 : Y profile (1 cm depth) at treatment distance for single field electron beam	37
Figure 9 : X profile (1 cm depth) at treatment distance for one dual-field electron beam	39
Figure 10 : Y profile (1 cm depth) at treatment distance for one dual-field electron beam	40
Figure 11 : Central axis PDD at treatment distance for dual-field electron beam.....	41
Figure 12 : Dose distribution for one dual-field electron beam on a cylindrical phantom	44
Figure 13 : Dose distribution for three dual-field electron beams on a cylindrical phantom	45
Figure 14 : Dose distribution for six dual-field electron beams on a cylindrical phantom	45
Figure 15 : PDD for single, three, and six dual-field electron beams on a cylindrical phantom	46
Figure 16 : Dose distribution for six dual-field electron beams on a cylindrical phantom with three arrows along 0, 30, and 60 degrees	48
Figure 17 : Central slice PDDs for six dual-field electron beams on a cylindrical phantom with three arrows along 0, 30, and 60 degrees shown in figure 16	48

Figure 18 : Dose distribution for six dual-field electron beams at central slice	50
Figure 19 : Dose distribution for six dual-field electron beams at off 40 cm from the central slice	50
Figure 20 : Dose distribution for six dual-field electron beams at off 80 cm from the central slice	51
Figure 21 : Off axis PDDs (0, 40, 80 cm off the central slice) on a 30 cm diameter cylindrical phantom	52
Figure 22 : The area of -10 cm to 10 cm from figure 21	52
Figure 23 : Dose distribution for six dual-field electron beams on a 20 cm diameter cylindrical phantom	53
Figure 24 : Dose distribution for six dual-field electron beams on a 30 cm diameter cylindrical phantom	54
Figure 25 : Dose distribution for six dual-field electron beams on a 40 cm diameter cylindrical phantom	54
Figure 26 : X profile (1 cm depth) for Vertex fields	57
Figure 27 : Y profile (1 cm depth) for Vertex fields	57
Figure 28 : X profile (1 cm depth) for Oblique field.....	58
Figure 29 : Y profile (1 cm depth) for Oblique field.....	59
Figure 30 : Dose distribution for combination of all fields on a cylindrical phantom.....	60
Figure 31 : PDD for 0, 30, and 60 degrees of profiles on a cylindrical phantom	60
Figure 32 : X profile for single electron beam from 300 to 550 cm SSD and dual-field electron beam	63
Figure 33 : X profile (1 cm depth) for these four configurations.....	63
Figure 34 : Y profile (1 cm depth) for these four configurations.....	64
Figure 35 : PDD for four filter configurations, dual-field electron beam, and single beam (550 cm SSD).....	65

Figure 36 : Composite PDD for four filter configuration, six dual-field electron beam,
and single open beam at 550 cm SSD.....66

Figure 37 : Surface dose from superior to inferior direction68

Figure 38 : X-ray contamination from superior to inferior direction68

Acknowledgements

I would like to take this opportunity to thank my advisor, Dr. Qiuwen Wu, for his time, support and guidance in all the steps of my research. I would also like to thank Dr. Gunasingha for offering computers for EGSnrc Monte Carlo simulations and Daren Sawkey for providing technical support for VirtuaLinac Monte Carlo simulations. I am grateful to my committee members, Dr. Christopher Kelsey, Dr. Rathnayaka Gunasingha, and Dr. Oana Craciunescu, for serving on my thesis committee and for providing insightful and valuable suggestions to me and this project.

I would also like to expend my deepest gratitude to my classmates in medical physics graduate program at Duke University and my parents for providing me with consistent supports and continuous encouragement throughout the years for my graduate study. This accomplishment would not have been possible without them.

1. Introduction

1.1 Total Skin Irradiation

Total skin irradiation (TSI) is a type of radiotherapy used to treat the entire body skin, and it is normally the effective treatment of mycosis fungoides which originate from the Cutaneous T-Cell Lymphoma. This special skin disease can be treated by several types of treatment including ultraviolet light, topical steroids, topical and systemic chemotherapies, local superficial radiotherapy and total skin irradiation. TSI is routinely pursued for patients who have a widespread skin disease, particularly in the setting of big plaque, tumor, or other therapies found effective. The low energy electron beam is used as the beam source within TSI since the low energy electron beam has a relatively shorter effective range than the high energy electron beam. The purpose of TSI is to deliver a homogeneous dose to the whole skin surface of a patient body at a limited depth while sparing the radiation dose delivered to the organ at risks (OARs). American Association of Physicists in Medicine Task Group 30 (AAPM TG-30 [1]) recommends $\pm 8\%$ in vertical (Superior to Inferior direction) uniformity and $\pm 4\%$ in horizontal uniformity (Left to Right direction) over 160 cm by 60 cm of the irradiated field.

1.2 Total Skin Irradiation Technique

Different types of technique have been developed for total skin irradiation. Per AAPM TG-30 [1], pairs of angled beams are used to deliver large fields to the entire skin of a patient body. The standard TSI procedure in our clinic is the stand-up technique

where dual-field electron beams are directed toward six different directions such as anterior-posterior (AP), posterior-anterior (PA), right anterior oblique (RAO), left anterior oblique (LAO), right posterior oblique (RPO), and left posterior oblique (LPO) positions with 60 degrees interval along the cranial-caudal axis at an extended source to skin (SSD) of 300 cm to get a full dose coverage of patient body. In the treatment of the stand-up technique, a patient receives six dual-field electron beams (12 single electron beams in total) in the first two fractions. Sequential two-day treatment cycle is involved in this special treatment after the first two fractions. That is, a patient receives three dual-field electron beams from AP, LPO, and RPO positions on the first day and receives other three beams from PA, LAO, and RAO positions on the second day to reduce the treatment time for each day. Multiple thermoluminescent dosimeters (TLDs) or optically stimulated luminescence dosimeters (OSLDs) are used to provide dosimetric data on the first day of the treatment, which allows the detection of dose inhomogeneities. Patient shieldings such as internal/external eye shields, mouth shield, hands shields, and feet shields are provided to prevent hot spot on these regions and to reduce the risk of other disease or side-effect during the treatment. Some underdosed regions such the soles of feet, shoulders, the perineal area, and the inframammary region in females require additional electron beams or low kilovoltage x-ray boost fields to get enough treatment dose.

In addition to a stand-up technique for total skin irradiation, a lay-down technique has been developed by Wu et.al [2] for patients who are too frail to stand in a certain position for a long time during the treatment. It is a good alternative for frail patients since patient safety is always the most important issue in a clinic. In this way, it can prevent frail patients from falling down during the treatment. A lay-down technique for total skin irradiation with a customized scatter filter based on Mayo clinic (Deufel et al. in 2013 [3]) is recently commissioned and implemented in our clinic. A scattering filter is mounted onto the accessory slot of the linac and used to improve dose uniformity, reduce patient setup time, and eliminate field junctions needed during the treatment. This scattering filter is constructed by 0.25 mm copper layer and two 0.1 cm polycarbonate plates, the detailed geometry of the scattering filter is shown in Figure 1.

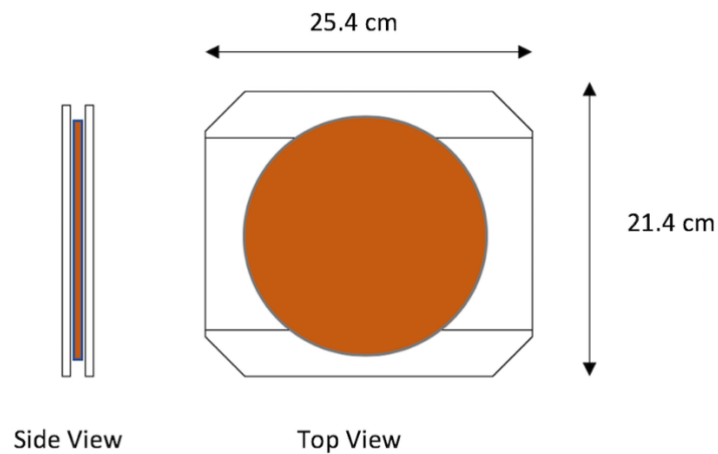


Figure 1 : Side view (Left) and top view (Right) of the customized copper filter

A patient lies down on a thin mat located under the gantry of the linac and receives three electron beams for vertex fields (AP and PA directions) at gantry angles of 0, 60, and 300 degrees to provide uniform dose for patient's superior to inferior direction. The thin mat is moved to be parallel to the waveguide of the linac for oblique fields and a patient receives a single electron beam for each position of oblique fields. This alternative technique for total skin irradiation demonstrates an acceptable dose uniformity and passes the uniformity of irradiation field requirements recommended by AAPM TG-30 [1].

1.3 Monte Carlo Method

Several non-standard measurements and dosimetric procedures are involved in total skin irradiation techniques and can be very time-consuming to develop and perform on a routine basis. Monte Carlo simulation can be used to validate the measured dosimetric data in this study. MC methods have been found to be a useful tool for reference and dosimetric calculations. It can be applicable from calculating the basic quantities of dosimetry to radiotherapy simulations. MC tool allows a user to simulate the detailed geometry of clinical linac, components of linac head such target, jaws, multi-leaf collimators (MLCs) and electron applicators, and arbitrary phantoms. Phase-space file which records the position, energy, and angular direction of particles passing through a scoring plane will be generated after MC simulation. This file then can be used to calculate three-dimensional (3D) dose distributions within an arbitrary phantom

made out of assigned materials. Two MC systems, EGSnrc and VirtuaLinac, were used in this study to validate the stand-up technique for total skin irradiation and the detailed method of these systems was described in section 2.

Monte Carlo methods have been applied to several research studies in total skin irradiation. Nevelsky et al. (2016) [4] [5] implemented an MC model using EGSnrc code to validate the dosimetric data for total skin irradiation, they also evaluated room scatter effects in total skin irradiation by MC methods. Furthermore, Pavon et al (2003) [6] verified the beam characteristics for large non-standard electron fields used for total skin irradiation by MC simulations. Ye et al. [7] applied MC methods to determine the design of beam modifier for total skin irradiation techniques. Accordingly, MC methods can be used to evaluate beam characteristics and dosimetric properties and it provides the most accurate dosimetric calculations in the radiation therapy field. However, there is always a trade-off between accuracy and computation time. That is, the limitation of MC methods for the total skin irradiation treatment is its long computation time since large scales of electron transport are involved in the MC simulations.

1.4 The Objectives of the study

Total skin irradiation technique is a complex procedure and there is no specific treatment system for this special technique. Therefore, the dosimetric data has to be measured by real experiments with customized devices in the clinic. Furthermore, as mentioned in section 1.3, there are several non-standard measurements and dosimetric

procedures involved in total skin irradiation techniques, so MC methods would be a useful tool for the dosimetric calculation. Therefore, the objectives of this research work aim to validate the dosimetric data by MC tools with the commissioning measured data for TSI stand-up technique in our clinic to evaluate if MC methods can become the foundation and guidance for investigation of future studies on technique optimizations.

Other than a point measurement, MC tools can provide further dosimetric information such as the full dose distribution of a patient phantom. Therefore, the second objective of this study is to perform the advanced dosimetric studies for the TSI stand-up technique using MC simulations. The dosimetric effect of different phantom sizes and off-axis effect were studied by analyzing the 3D dose distribution on a cylindrical phantom.

The third objective of this study is to optimize/modify the currently available TSI stand-up technique to improve the dose uniformity and efficiency of treatment procedures. For example, a customized copper filter (scattering filter) is mounted on the linac to improve the uniformity of dose and to eliminate the junction fields needed in the TSI lay-down technique. We are thinking of using different materials and filter designs to eliminate the dual-field electron beam needed in a TSI stand-up technique. With a scattering filter mounted, an equivalent dose uniformity as the dual-field electron beam in stand-up technique could be achieved with a single electron beam only. That is, the

standard stand-up technique for TSI could be implemented with a single electron beam if the scattering filter is used.

2. Material and Methods

The measured data in this study was recorded during TSI commissioning for the stand-up technique in our clinic, and several measurements were done such as the output factor (OF) at 100 cm SSD (isocenter), output factor at the SSD of treatment distance, investigation of the optimal gantry angle, vertical and horizontal beam profiles at both isocenter and the treatment distance, percentage depth dose (PDD), x-ray contamination, and body factor (B-factor) which relates the skin dose for six directions to the dose for single direction. MC simulations were performed with EGSnrc-based codes (BEAMnrc and DOSXYZnrc) and Geant4-based VirtuaLinac. The MC model in the EGSnrc environment has to be built by the user itself such as the geometry of the linac and the components of the linac head needed in TSI treatment, while the MC model of VirtuaLinac has been implemented by Varian for the simulation of the TrueBeam linac. The methods for the commissioning measurement and MC simulations in both EGSnrc and VirtuaLinac were described in detail from 2.1 to 2.2.

2.1 Commissioning Measurement at Duke Radiation Oncology

Measurements in this study were carried out using a Varian TrueBeam STX Linac in 6HDTSE mode (High dose rate mode) which stands for 6 MeV and 2500MU/min. In this study, X profile is superior to inferior direction of a patient; Y profile is left to right direction of a patient; and Z profile is anterior to posterior direction of a patient.

2.1.1 TSI Stand-up Technique

In the TSI stand-up technique at our clinic, jaws settings (X jaw and Y jaw) are 36x36 cm², collimator angle is 0 degrees, and gantry angles are tilted ± 19 degrees (289 and 251 degrees) for a dual-field electron beam with the treatment distance of 300 cm SSD.

To determine the output factor at isocenter, a plane-parallel ion chamber (PTX 34001) was used to measure the output in terms of cGy per MU in a flat solid water phantom at reference conditions which were field size of 36x36 cm², SSD of 100 cm, at depth of 1.5 cm without electron applicator. Since the optimal gantry angle was machine and geometry dependent for the TSI stand-up technique, the flatness of the vertical beam profiles and x-ray contamination were measured for each gantry angle from 16 to 20 degrees in our clinic to evaluate the optimal rotated angle of the gantry for this specific machine.

At the treatment distance of 300 cm SSD, the X and Y profiles were measured at 1 cm depth by vertically and horizontally moving the TSI rotating platform and adding/removing the styrofoam with various thicknesses. Once gantry angle has been optimized (19 degrees is used in our clinic for this specific machine), the X and Y beam profiles for both single electron beam and dual-field electron beam at gantry angle of 289 and 251 degrees were measured at the treatment distance. The flatness of the X and Y profiles for dual-field electron beam were evaluated.

PDD profiles were measured by adding/removing plates of solid water with various thicknesses for one dual-field electron beam and six dual-field electron beams at the treatment distance. The absolute dose for one dual-field electron beam was measured at the depth of the surface at the treatment distance. The output factor at the depth of surface at the treatment distance was calculated as the ratio of the surface dose at the treatment distance to the surface dose at the depth of reference (d_{ref}) at isocenter. The depth of maximum, R_{50} which is the depth when radiation dose drops to 50% of its maximum value, and x-ray contamination which is defined as the dose at the depth of 10 cm were determined by PDD profiles using films and a cylindrical phantom. Two-dimensional (2D) transversal dose distribution of one dual-field electron beam and six dual-field electron beams were measured on a 30 cm diameter cylindrical phantom.

To obtain more precise x-ray contamination and B-factor, defined as a ratio of the surface dose from six treatment directions to the surface dose from single treatment direction, in a patient body, an anthropomorphic phantom was placed on the TSI rotating platform at the treatment distance. EDR2 films were located between the slices of the phantom at different locations: upper thigh, head, neck, mid-mediastinum, and central axis to measure the 2D transversal dose distribution at different locations. OSLDs were also placed at the surface of an anthropomorphic phantom to measure the surface dose for one dual-field electron beam and six dual-field electron beams, which were then used to calculate the B-factor. This B-factor is an important factor that it takes into

account the radiation dose to a point of the patient while rotating and receiving radiation dose from all treatment directions.

2.1.2 TSI Lay-down Technique

In the TSI lay-down technique at our clinic, jaws settings (X jaw and Y jaw) are 30x40 cm², collimator angle is 0 degree for vertex fields and 90 degrees for oblique fields, gantry angles are 0, 60, and 300 degrees for vertex fields, and 270 degrees for oblique fields, and the treatment distance is 195 cm and 305 cm equivalent SSD for vertex and oblique fields respectively. The customized copper filter is mounted onto the accessory slot of the linac for both vertex and oblique fields.

At the treatment distance of vertex fields, the X and Y profiles at the depth of 1 cm were measured with the gantry angle of 0, 60, and 300 degrees. The optimized weighting factor to combine these fields was 0.22 (0 degrees) : 1.0 (60 degrees) : 1.0 (300 degrees) to maximize the flatness of X profiles at the depth of 1 cm. At the treatment distance of oblique fields, X and Y profiles at the depth of 1 cm were measured at gantry angle of 270 degrees. PDDs for both vertex fields and oblique fields were measured and used to determine d_{max} , R_{80} , R_{50} , and x-ray contamination.

The dose at the depth of 1.5 cm at isocenter for the open field was measured as a reference and used to determine the relative output factors for both vertex fields and oblique fields. EBT3 films were stitched together and placed between the halves of a 30 cm diameter cylindrical phantom and an anthropomorphic phantom to measure the

surface dose and x-ray contamination. OSLDs were also placed on the surface and the center of an anthropomorphic phantom to measure the dose for vertex fields and oblique fields. These dose values then were used to calculate the ratio of surface dose from all beams combined to a single beam to obtain equivalent B-factors for vertex and oblique fields.

2.2 Monte Carlo Simulations

2.2.1 EGSnrc

The EGSnrc (Electron Gamma Shower) is an MC toolkit that can be used to simulate the coupled transport of electrons and photons in an arbitrary geometry for particles energies from 1 keV to 10 GeV. It was originally developed at the Stanford Linear Accelerator Center (SLAC) and currently maintained by National Research Council of Canada. EGSnrc had been the standard MC simulation system used in the radiation therapy field. EGSnrc-based codes, BEAMnrc and DOSXYZnrc were used in the downstream of the phase-space plane. BEAMnrc was used to simulate the transport of particles, component modules (CM) such as beam source, X and Y jaws, and multi-leaf collimators (MLC) needed as in TSI treatment. The MC model was built to simulate the unit of radiotherapy treatment and a scoring plane at the distance of interest (either at isocenter or the treatment distance) was included to record all the necessary information such as position, energy, and direction of particles traveling through it and

eventually store particles information in a phase-space file after the MC simulation. This generated phase-space file can then be used as an input within DOSXYZnrc which deposits energy in a designed phantom to calculate three-dimensional (3D) dose distribution.

IAEA compatible formatted phase-space files provided by the linac vendor were placed below the ion chamber and above X and Y jaws. Multiple validated phase-space files were collected and converted into a huge phase-space file containing around 7.5×10^8 particles to avoid recycling particles during the MC simulations. This huge phase-space file was used as the main source within BEAMnrc and placed 26.7 cm away from the beam target. CMs of Jaws was included in the MC model for the TSI stand-up technique with the accurate materials and geometry obtained from the TrueBeam Monte Carlo package version 1.1 available at www.MyVarian.com. The additional customized copper filter for the TSI lay-down technique was simulated by the CMs of SLAB and FLATFILT in the MC model. Electron production cutoff (AE) and bremsstrahlung production cutoff (AP) were 0.521 MeV and 0.01 MeV. Photon global cutoff energy (PCUT) and electron global cutoff energy (ECUT) were 0.01 MeV and 0.521 MeV for the accurate low-energy simulation. Electron range rejection (ESAVE GLOBAL of 1 MeV) was an effective method to speed up the computation time during the MC simulation.

2.2.1.1 Validate the dosimetric data at isocenter

To validate the MC model at isocenter for the open beam (for TSI stand-up technique), jaws settings of $36 \times 36 \text{ cm}^2$, $40 \times 40 \text{ cm}^2$ and $30 \times 40 \text{ cm}^2$ were first tested and the parameters of the MC model were first tuned to match the TSI commissioning measurements. The dosimetric quantities: PDD, X and Y profiles were compared and used to validate the MC model for the stand-up technique. A secondary phase-space file was generated at isocenter when particles traveling through a scoring plane placed at isocenter. This file can be used as an input in DOSXYZnrc to calculate 3D dose distribution and a .3ddose file was generated. 3D dose distribution can be extracted from the .3ddose file and analyzed by the MATLAB code.

To validate the MC model at isocenter for the filtered beam (with scattering filter for TSI lay-down technique), jaws settings of $10 \times 10 \text{ cm}^2$, $20 \times 20 \text{ cm}^2$, $30 \times 30 \text{ cm}^2$, $40 \times 40 \text{ cm}^2$, and $30 \times 40 \text{ cm}^2$ were tested and evaluated the dosimetric effect of the scattering filter. The parameters of the MC model were first tuned to match the commissioning measurement. The dosimetric quantities: PDD, X/Y profiles were compared and used to validate the MC model for the lay-down technique. A secondary phase-space file was generated at isocenter when particles traveling through a scoring plane placed at isocenter. This file can be used as an input in DOSXYZnrc to calculate 3D dose distribution.

2.2.1.2 Validate the dosimetric data at treatment distance for the Stand-up technique

Once the MC model has been validated at isocenter, a secondary phase-space file generated at isocenter was rotated at gantry angle where was located 19 degrees and -19 degrees in relation to the axis, which was perpendicular to the patient and then used as a beam source within BEAMnrc to further simulate the particles transport at the treatment distance. A scoring plane was placed at the treatment distance and a phase-space file was generated and then used in DOSXYZnrc to calculate 3D dose distribution in a 200x200x10 cm³ water phantom with a voxel size of 2x2x0.1 cm³ and a diameter of 30 cm cylindrical phantom with a voxel size of 0.1x2x0.1 cm³ for both single and six dual-field electron beams. The .3ddose files generated by DOSXYZnrc can be read by the MATLAB code to extract 3D dose distribution and calculate PDDs, profiles, output factors, x-ray contamination, and B-factor. Different sizes of the cylindrical phantom (20, 30, and 40 cm diameters) were also simulated to evaluate the dosimetric effect of different sizes of patients. Figure 2 shows a general workflow of EGSnrc.

2.2.1.3 Validate the dosimetric data at treatment distance for the Lay-down technique

Once the MC model has been validated at isocenter, a secondary phase-space file generated at isocenter was rotated 0, 60 and 300 degrees for vertex fields and 270 degrees for oblique fields to simulate the rotated fields in the lay-down technique. A scoring plane was placed at the treatment distance and a phase-space file was generated and then used in DOSXYZnrc to calculate 3D dose distribution in a 200x200x10 cm³

water phantom with a voxel size of $2 \times 2 \times 0.1 \text{ cm}^3$ and a diameter of 30 cm cylindrical phantom with a voxel size of $0.1 \times 2 \times 0.1 \text{ cm}^3$ for both vertex and oblique fields. The .3ddose files generated by DOSXYZnrc can be read by a MATLAB code to extract and calculate PDDs, profiles, output factors, x-ray contamination, and B-factor. Different sizes of the cylindrical phantom (20, 30, and 40 cm diameters) were also simulated to evaluate the dosimetric effect of different sizes of patients.

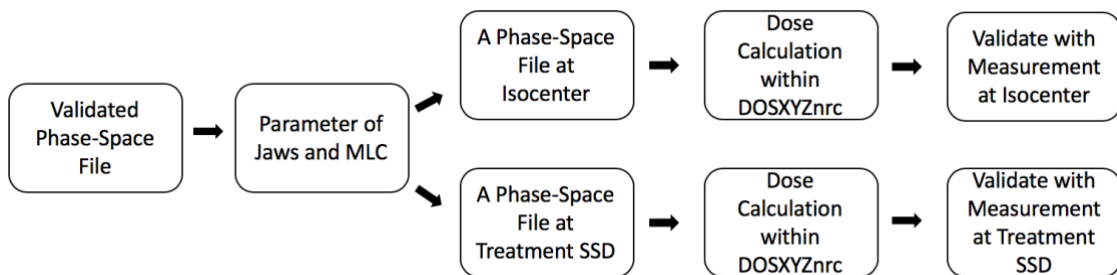


Figure 2 : A general workflow of EGSnrc

2.2.1.4 Investigation of effect of filter design for the TSI Stand-up technique

In the standard stand-up technique for total skin irradiation, a pair of overlapping beams (dual-field electron beam) is required to cover the whole length of the patient. The use of a scattering filter made out of the material with high atomic number (high Z) placed at accessory slot can eliminate the use of dual-field electron beam in the standard TSI stand-up treatment, with comparable dosimetric

characteristics. This can improve the uniformity of treatment field, eliminate field junctions needed and improve the efficiency of the treatment.

The material (Cu, Zn, Fe, Au, and Ag) were chosen because of their stability and availability. The thickness ranges from 0.05 mm to 0.55 mm, depending on the characteristics of the material. The SSD from 250 cm to 350 cm were studied. For each material, we vary the thickness and SSD, to evaluate the following quantities: PDD, profiles and output at depth of maximum, and compared them with the standard dual-field electron beam at the treatment SSD that has been used in the clinic.

MC simulations were performed within the EGSnrc environment. CM of SLAB and FLATFILT were used to simulate the scattering filter mounted at the accessory slot of the linac in the MC model. Jaws setting were 30x40 cm² and collimator angle was 90 degrees. Phase-space files generated at 250, 300, 325, and 350 cm SSD were used as the inputs within DOSXYZnrc to calculate the 3D dose distribution in a flat solid water phantom. A 30 cm diameter cylindrical phantom was also built for evaluating the composite dose distribution of each acceptable configuration.

2.2.2 VirtuaLinac

VirtuaLinac, a cloud-based system utilizing Geant4 Monte Carlo code to simulate the treatment head of the Varian TrueBeam linac accelerator, implements the detailed linac head geometry and material models, validated phase space files, and a voxelized phantom. To launch a VirtuaLinac MC simulation, the user has to request an available

spot on Amazon cloud to reserve a virtual server that can run MC applications. The input of VirtuaLinac is expanded to include an XML (Extensible Markup Language) file and API.py (Application Programming Interface) to specify the beam parameters, control the gantry rotation, and MU delivery. After the VirtuaLinac MC simulation finished, a .dose file containing the information of 3D dose distribution will be generated and it can be read by the MATLAB code to extract the 3D dose distribution and calculate the dosimetric quantities. Figure 3 shows a general workflow of VirtuaLinac.

In this study, VirtuaLinac served as a secondary check for the results from EGSnrc. The same phase-space files provided by Varian and previously validated were used in MC simulations for both EGSnrc and VirtuaLinac. In VirtuaLinac, parameter settings of jaws, MLC, collimator angle, and SSD were determined based on the treatment setup in the TSI stand-up technique. In order to validate the stand-up technique, gantry angles from 16 to 20 degrees were simulated and 3D dose distributions for each gantry angle were calculated on a flat solid water phantom which was $200 \times 200 \times 10 \text{ cm}^3$ with a voxel size of $2 \times 2 \times 0.1 \text{ cm}^3$ and a 30 cm diameter cylindrical phantom with a voxel of $0.1 \times 2 \times 0.1 \text{ cm}^3$ built by a python code, and compared the dosimetric quantities with measured data and the MC results from EGSnrc.

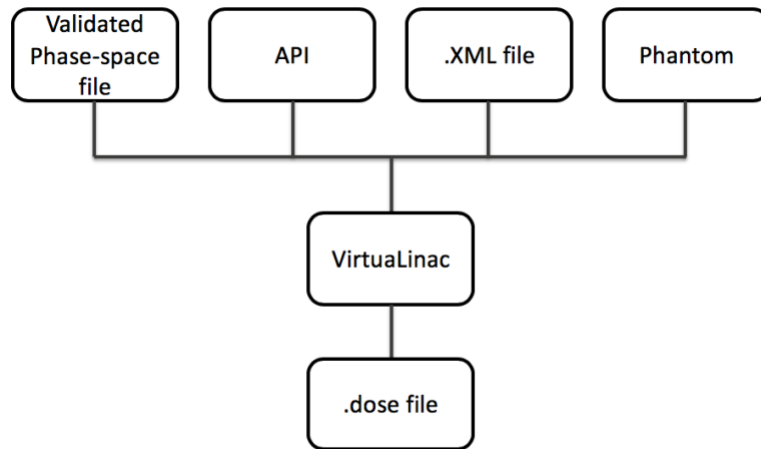


Figure 3 : A general workflow of VirtuaLinac

3. Results and Discussion

Again, X profile is from a patient's superior to inferior direction; Y profile is from a patient's left to right direction; and Z profile is from a patient's anterior to posterior direction in this study. The X and Y profiles in this section were all plotted at 1 cm depth of the phantom. The average d_{max} was determined by averaging the 99 % to 100 % D_{max} .

The X/Y profiles, PDD, and dose distributions demonstrated from Figure 1 to 15 and Table 1 to 5 were provided here to validate the TSI stand-up technique. Figure 16 to 25 and Table 6 to 7 were demonstrated the advanced dosimetric studies for the TSI stand-up technique using MC method. The validation of the TSI lay-down technique was only described with the main results from EGSnrc MC simulations and the measured data (Figure 26 to 31). The detailed study for the TSI lay-down technique was covered and can be acquired from Ruiqi Li's master thesis with title "Validation of the dosimetry for a lay-down Total Skin Irradiation Techniques by Monte Carlo Simulation [10]". The results for the investigation of filter effect in the stand-up technique were shown in Figure 32 to 38 and Table 8 to 9.

3.1 Validation of Monte Carlo Simulation at 100 cm SSD

Figure 4 shows the X profiles at 1 cm depth at 100 cm SSD for both measured and simulated data. The average difference for EGSnrc was within 1.9 % (with the maximum 5 % difference), while the average difference for VirtuaLinac was within 1.7 % (with the

maximum 4 % difference), compared with the measured data. As can be seen, both MC systems showed a good agreement with the measured data, the maximum difference for both MC systems was at ± 15 cm off from the central axis.

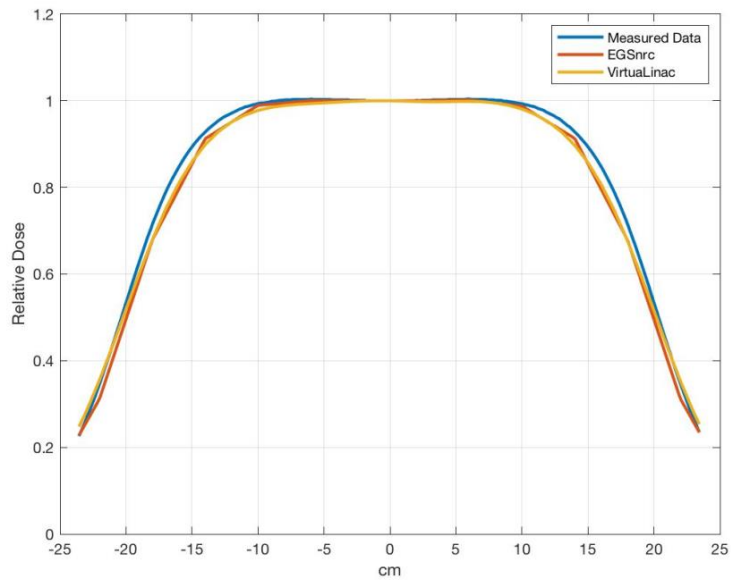


Figure 4 : X profile (1 cm depth) of 36x36 cm² field size at isocenter

Figure 5 shows the Y profiles at 1 cm depth at 100 cm SSD for both measured and simulated data. The average difference for EGSnrc was within 1.8 % (with the maximum 5 % difference), while the average difference for VirtuaLinac was 1.2 % (with the maximum 5 % difference), compared with the measured data. As can be seen, both MC tools showed good agreements with the measured data, the maximum difference for both MC systems was at ± 15 cm from the central axis.

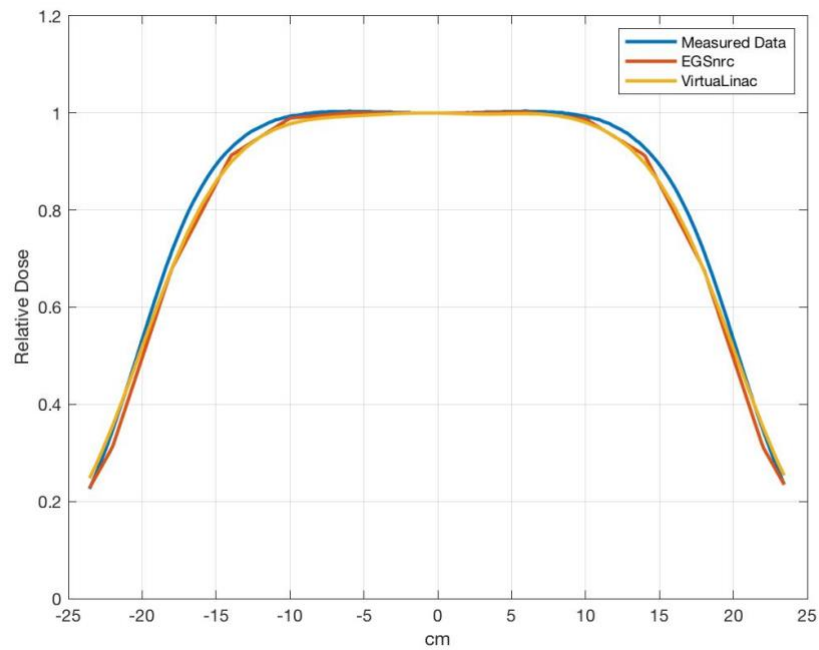


Figure 5 : Y profile (1 cm depth) of 36x36 cm² field size at isocenter

Figure 6 showed the central axis PDD at 100 cm SSD with 36x36 cm² field size for both measured and simulated data. The detailed dosimetric quantities were listed in Table 1. The differences for average d_{max} , R_{50} , and R_{80} in EGSnrc and VirtuaLinac were all within 1 mm, compared with the measured data.

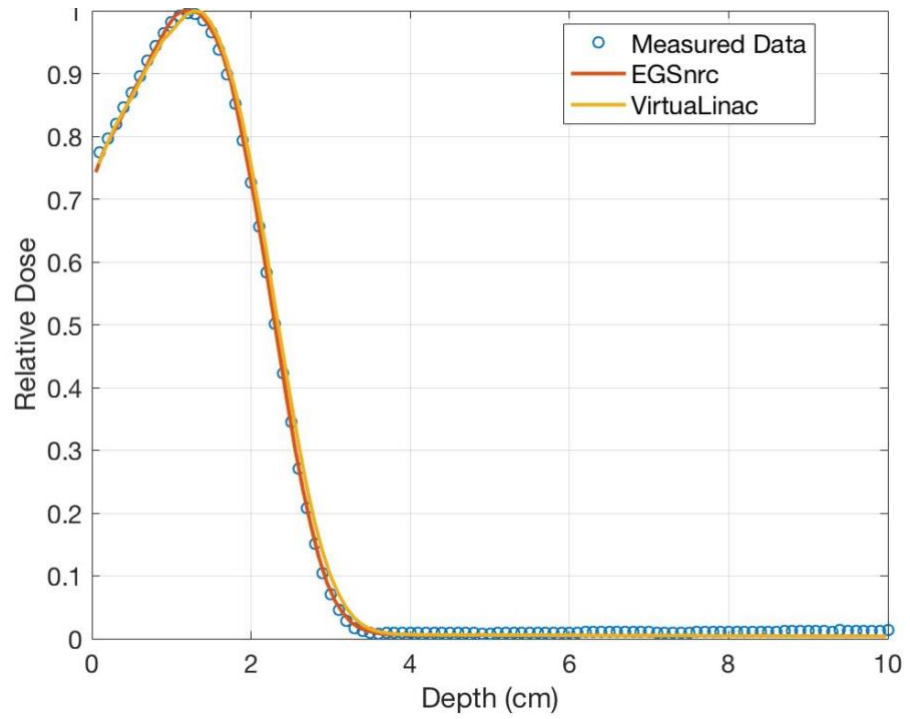


Figure 6 : Central axis PDD of 36x36 cm² field size at isocenter

Table 1 : Dosimetric quantities of central axis PDD with 36x36 cm² field size at isocenter

Open field 100 cm SSD	Measured data	EGSnrc	VirtuaLinac
Average d_{max} (cm)	1.20	1.21	1.23
R_{50} (cm)	2.27	2.30	2.31
R_{80} (cm)	1.87	1.89	1.90

3.2 Validation of Monte Carlo Simulation at 300 cm SSD for the Stand-up technique

3.2.1 Profiles for single-field electron beam (-19 degrees)

Figure 7 shows the X profiles at 1 cm depth at treatment distance for both measured and simulated data. The average difference for EGSnrc was within 1.4 % (with the maximum 4 % difference), while the average difference for VirtuaLinac was within 1 % (with the maximum 2 % difference), compared with the measured data. As can be seen in Figure 5, VirtuaLinac had a relatively better agreement with the measured data than EGSnrc. EGSnrc had a maximum 4 % difference at -40 to 0 cm.

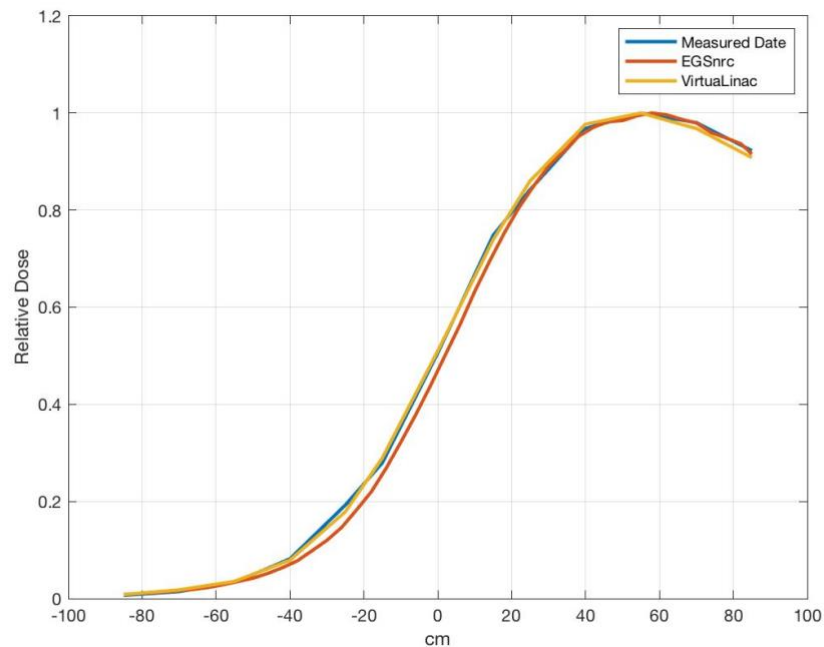


Figure 7 : X profile (1 cm depth) at treatment distance for single field electron beam

Figure 8 shows the Y profiles at 1 cm depth at 300 cm SSD for both measured and simulated data. The average difference for EGSnrc was within 1 % (with the maximum 2 % difference), while the average difference for VirtuaLinac was within 1.7 % (with the maximum 3.7 % difference), compared with the measured data.

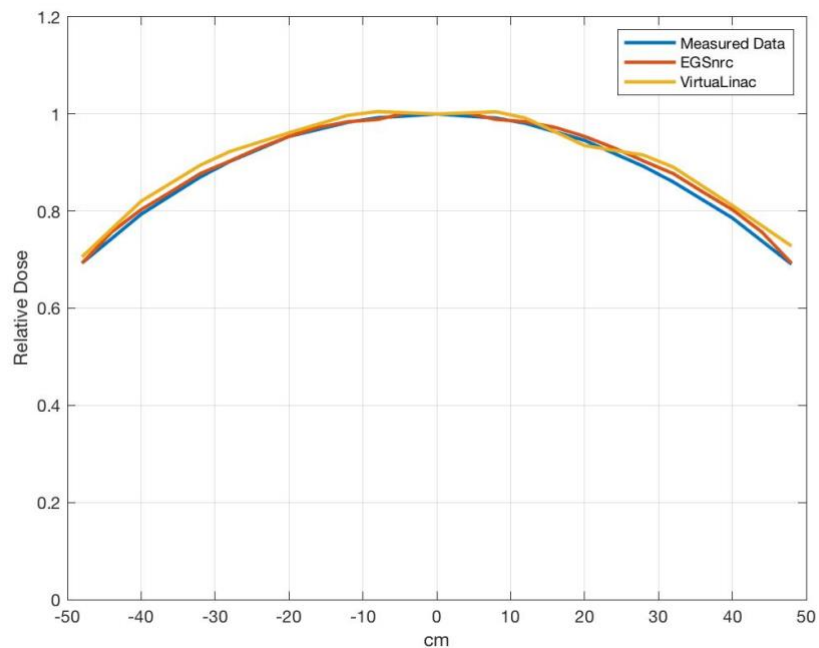


Figure 8 : Y profile (1 cm depth) at treatment distance for single field electron beam

Table 2 lists the dosimetry quantities of central axis PDD at 300 cm SSD for both measured and simulated data. The differences for average d_{max} and R_{50} in EGSnrc and VirtuaLinac were within 1 mm, compared with the measured data, while there were within 1 mm and 2 mm difference in R_{80} for VirtuaLinac and EGSnrc respectively.

Table 2 : Dosimetric quantities of central axis PDD at treatment distance for single field electron beam

Single electron beam	Measured data	EGSnrc	VirtuaLinac
Average d_{\max} (cm)	1.00	1.09	1.07
R_{50} (cm)	2.05	2.10	2.06
R_{80} (cm)	1.55	1.71	1.61

3.2.2 Profiles for dual-field electron beam (± 19 degrees)

Figure 9 shows the X profiles at 1 cm depth at 300 cm SSD for both measured and simulated data for dual 6 MeV electron. The average difference for EGSnrc was within 5.5 % (with the maximum 8.6 % difference), while the average difference for VirtuaLinac was within 1 % (with the maximum 2 % difference), compared with the measured data. As can be seen in Figure 9, VirtuaLinac has a better agreement with the measured data than EGSnrc. This huge differences in EGSnrc may be caused by the rotation of gantry in BEAMnrc code, this problem is currently under investigation.

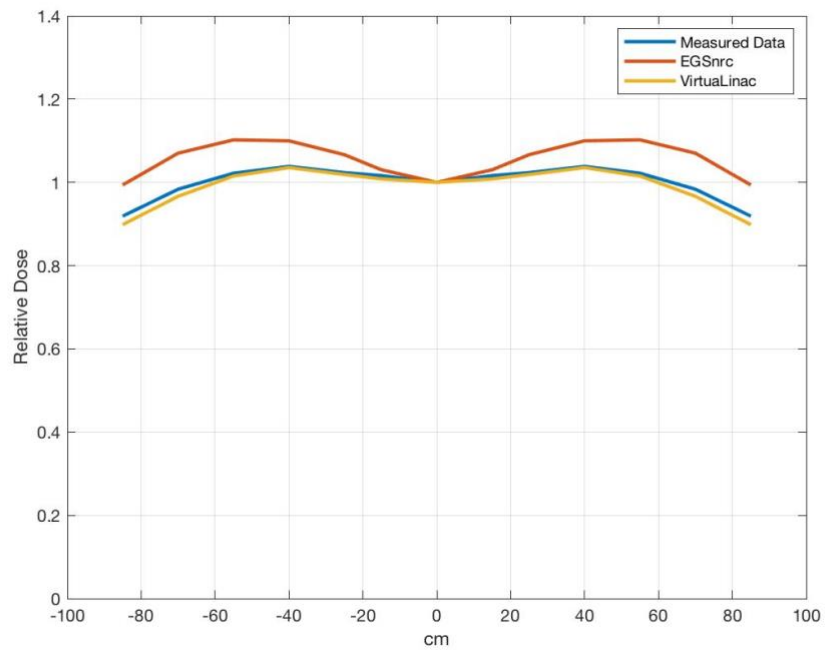


Figure 9 : X profile (1 cm depth) at treatment distance for one dual-field electron beam

Figure 10 shows the Y profiles at 1 cm depth at 300 cm SSD for both measured and simulated data for dual 6 MeV electron. The average difference for EGSnrc was within 1 % (with the maximum 1.6 % difference), while the average difference for VirtuaLinac was within 1 % (with the maximum 2.4 %), compared with the measured data. Although EGSnrc didn't perform well in X profile, it matched the measured data well in the Y profile.

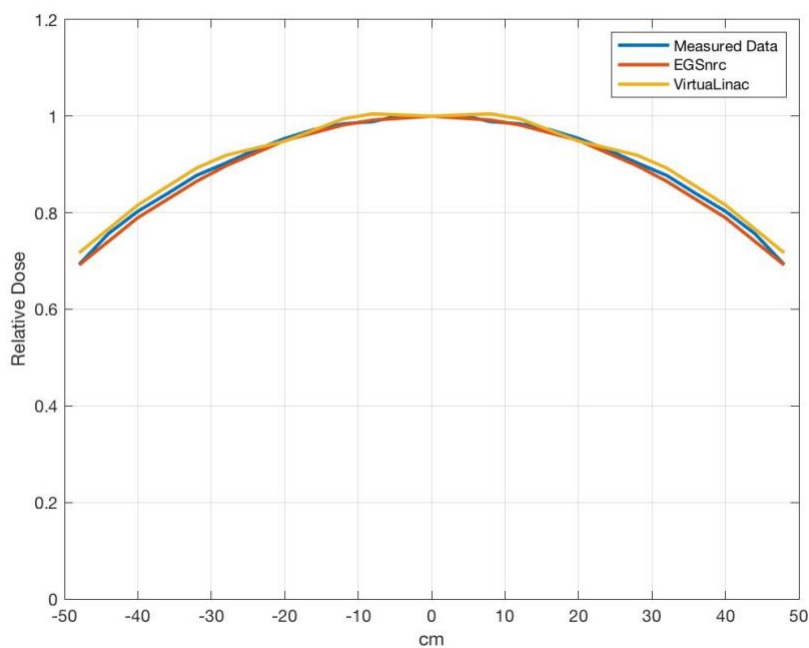


Figure 10 : Y profile (1 cm depth) at treatment distance for one dual-field electron beam

Figure 11 shows the central axis PDD at 300 cm SSD for both measured and simulated data for dual-field electron beam. The detailed dosimetric quantities were listed in Table 3. The average depth of maximum was 1.08 cm (0.95-1.2 cm) in EGSnrc and 1.07 cm (0.95-1.19 cm) in VirtuaLinac, compared with the measured data of 1.00 cm. R_{50} for EGSnrc and VirtuaLinac were 2.10 cm and 2.06 cm, which generally agreed with the measured data of 2.07 cm. There were within 2 mm differences in R_{50} for both EGSnrc and VirtuaLinac, compared with the measured data. The x-ray contamination in a 30 cm diameter cylindrical phantom for the measured data, EGSnrc, and VirtuaLinac

were all very small (less than 1 % D_{max}). The output factor at the surface for the measured and simulated data were similar. This output factor can tell you how many MU are needed if you want to deliver the same amount of radiation dose.

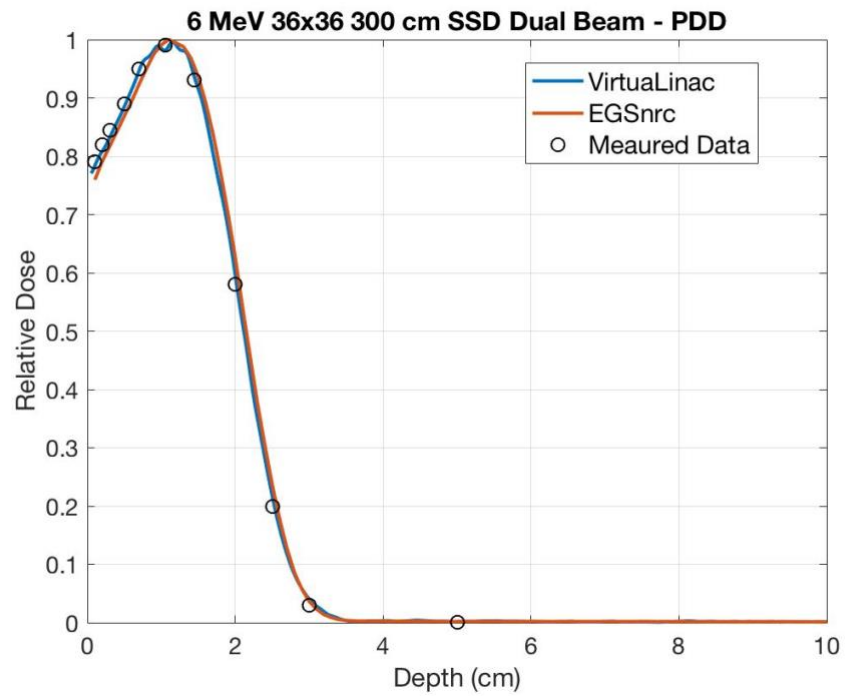


Figure 11 : Central axis PDD at treatment distance for dual-field electron beam

Table 3 : Dosimetric quantities of PDD at treatment distance for one dual-field electron beam

Dual-field electron beam	Measured Data	EGSnrc	VirtuaLinac
Average d_{\max} (cm)	1.00	1.08	1.07
R_{50} (cm)	2.07	2.10	2.06
R_{80} (cm)	1.58	1.71	1.61
Output factor at surface (cGy/MU)	0.072	0.071	0.070
# MU to get 150 cGy	2083	2113	2143

3.2.3 Dose distribution on a cylindrical phantom for the stand-up technique

3.2.3.1 Composite PDD for single, three, and six dual-field electron beams on a cylindrical phantom

Table 4 lists the dosimetric quantities of the composite PDD at 300 cm SSD on a cylindrical phantom for both measured and simulated data for six dual-field 6 MeV electron beams. When six dual-field electron beams were combined and calculated the 3D dose distribution on a 30 diameter cylindrical phantom, depth of maximum was 1.4 mm (1 - 1.8 mm) in EGSnrc and 1.5 mm in VirtuaLinac (1.1 - 1.8 mm), compared with the measured value of 1.6 mm. X-ray contamination for EGSnrc and VirtuaLinac were 1.2 % D_{\max} and 1.3 % D_{\max} respectively, compared with the measured value of 2 % D_{\max} .

Table 4 : Dosimetric quantities of PDD at treatment distance for six dual-field electron beams

Six dual-field electron beams	Measured Data	EGSnrc	VirtualLinac
Average d_{\max} (mm)	1.6	1.4	1.5
X-ray contamination (% D_{\max})	2.0	1.2	1.3

In the EGSnrc MC simulation on a 30 cm diameter cylindrical phantom, Figure 12 shows the dose distribution for one dual-field electron beam in a TSI stand-up technique. As mentioned in previous sections, in the sequential two-day treatment cycle, a patient receives three dual-field electron beams from AP, LPO, and RPO positions in the first day and receives other three dual-field electron beams from the other positions. Figure 13 shows the dose distribution for a patient receiving three dual-field electron beams after one-day treatment. Figure 14 demonstrates the dose distribution for the combination of all six dual-field electron beams after a sequential two-day treatment. You can notice that the d_{\max} shifts toward the surface of the cylindrical phantom when the number of dual-field electron beam increases (from single to six dual-field). This phenomenon can be clearly seen in the PDD curve plotted in Figure 15. The d_{\max} was 1.10 cm for single dual-field; 0.14 cm for six dual-field. That is, d_{\max} shifted 0.96 cm toward the surface of the cylindrical phantom, which is the purpose of this technique that a uniform dose is delivered to a limited depth of the surface. The surface dose was 97 %

for six dual-field electron beams, compared to 78 % for single dual-field. Table 5 lists the detailed dosimetric quantities for single, three, six dual-field electron beams.

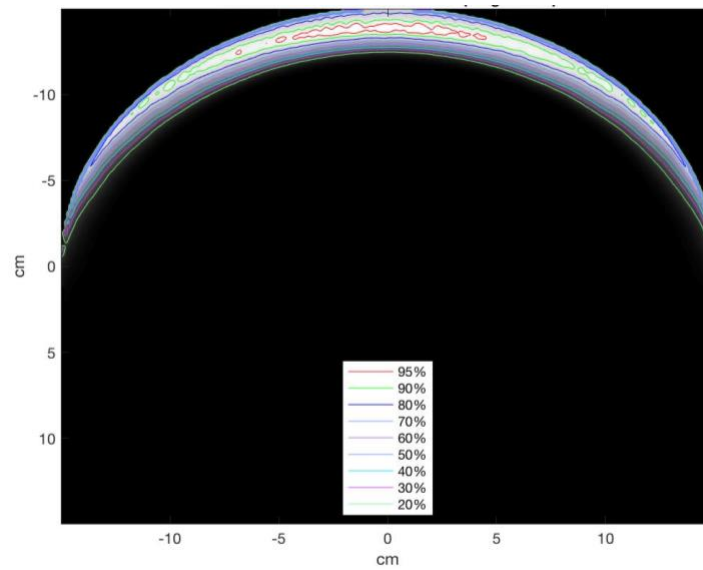


Figure 12 : Dose distribution for one dual-field electron beam on a cylindrical phantom

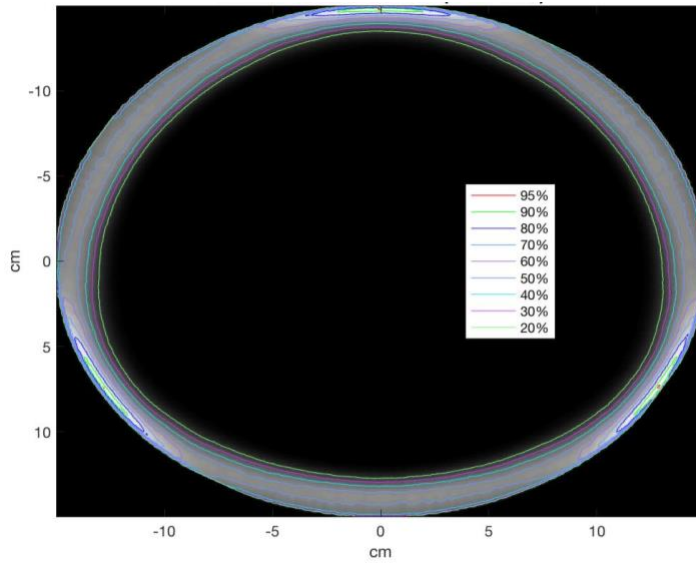


Figure 13 : Dose distribution for three dual-field electron beams on a cylindrical phantom

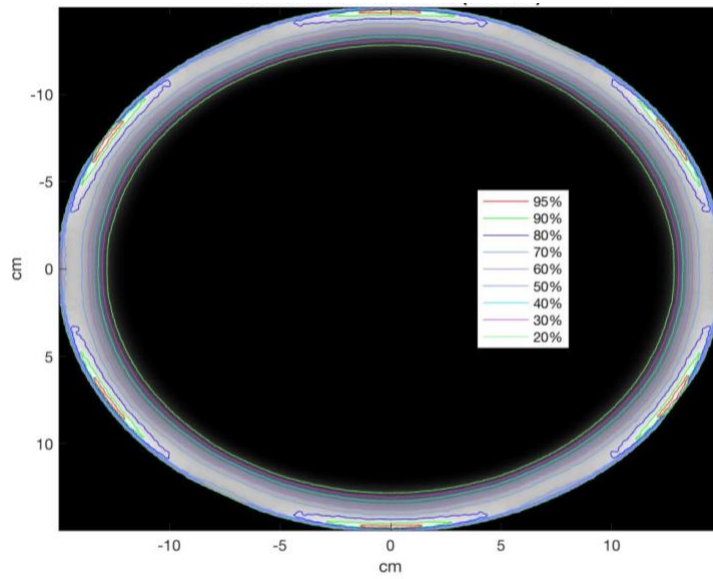


Figure 14 : Dose distribution for six dual-field electron beams on a cylindrical phantom

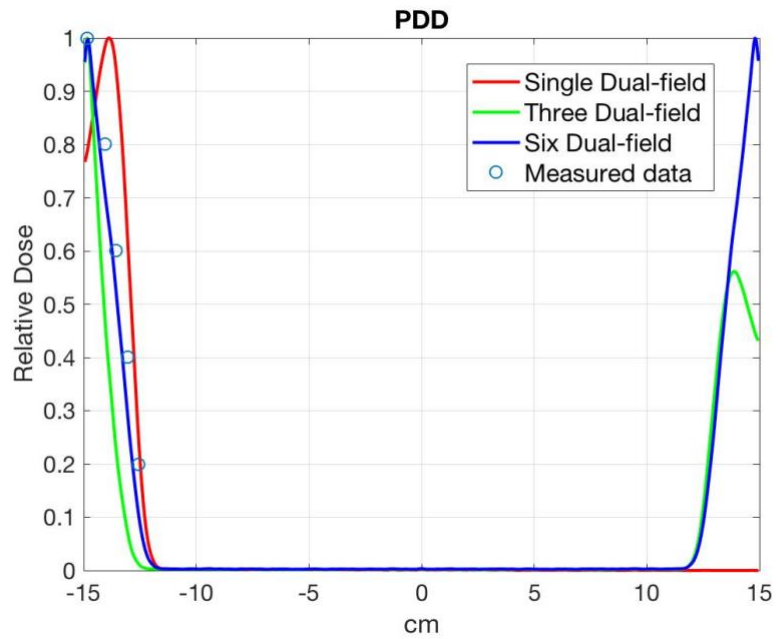


Figure 15 : PDD for single, three, and six dual-field electron beams on a cylindrical phantom

Table 5 : Dosimetric quantities for single, three, six dual-field electron beams at central slice of 30 cm diameter cylindrical phantom

Central Slice	d_{\max} (cm)	Surface dose (%)	R_{80} (cm)
Single dual-field	1.10	78	1.68
Three dual-field	0.15	97 / 44	0.44
Six dual-field	0.14	97	0.65

3.2.3.2 Composite PDD along 0, 30, and 60 degree for six dual-field electron beams on a cylindrical phantom

As can be noticed in Figure 14, in the dose distribution for six dual-field electron beams, there are some hot areas (AP, PA, LAO, RAO, LPO, and RPO) and cold areas, so the PDDs were plotted along the three arrows (shown in figure 16) to evaluate the dosimetric quantities of these hot and cold areas. Figure 17 shows the PDD of the central slice of a cylindrical phantom for three arrows along 0, 30, and 60 degrees shown in figure 16. The PDDs along 0 and 60 degrees basically showed the same curve with a little different on the surface dose, this might cause by the variation of rotation in the MATLAB code. However, the PDD along 30 degrees showed a huge difference from PDDs along 0 and 60 degrees. The surface dose along 30 degrees was 53 %, compared with 97 % for 0 degrees. The detailed dosimetric quantities were shown in Table 6.

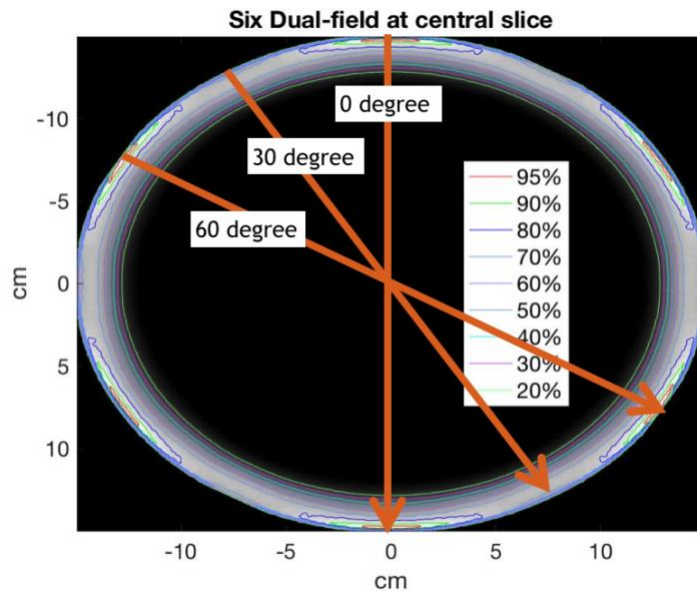


Figure 16 : Dose distribution for six dual-field electron beams on a cylindrical phantom with three arrows along 0, 30, and 60 degrees

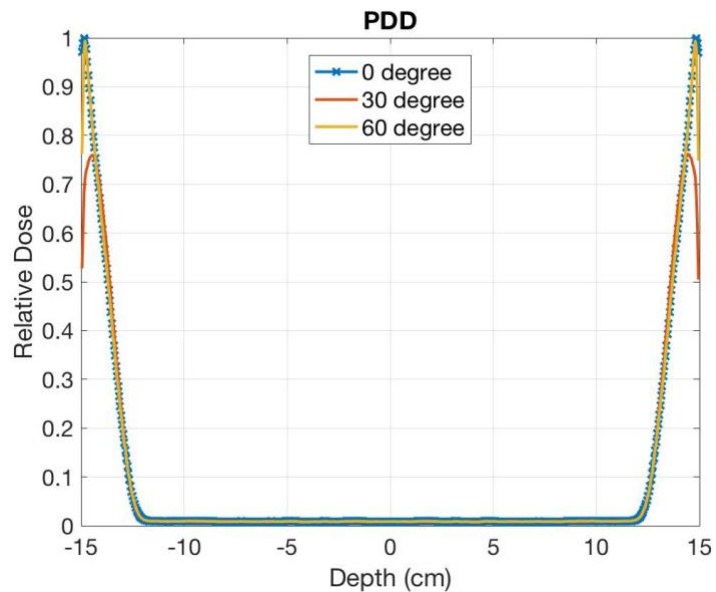


Figure 17 : Central slice PDDs for six dual-field electron beams on a cylindrical phantom with three arrows along 0, 30, and 60 degrees shown in figure 16

Table 6 : Central slice PDDs along 0, 30, 60 degrees arrows shown in figure 16

Central slice	d_{\max} (cm)	Surface dose (%)
0 degree	0.14	97
30 degree	0.45	53
60 degree	0.15	76-97

3.2.3.3 Off axis PDD (0, 40, 80 cm from the central slice) for six dual-field electron beams on a cylindrical phantom

Figure 18, 19, and 20 show the composite dose distribution at the central slice, off 40 cm from the central slice, and off 80 cm from the central slice respectively on a 30 cm diameter cylindrical phantom. The PDDs were plotted and shown in figure 21, these three PDD curves showed a similar surface dose and d_{\max} , the most different among the dosimetric quantities was the x-ray contamination. You can have a closer look at this difference in figure 22. The x-ray contamination tends to become higher when the off-axis distance increases. This might be caused by the dual-field electron beam used in the TSI stand-up technique. The angled beams have spared the x-ray contamination at the central region and moved the higher x-ray contamination to the edges.

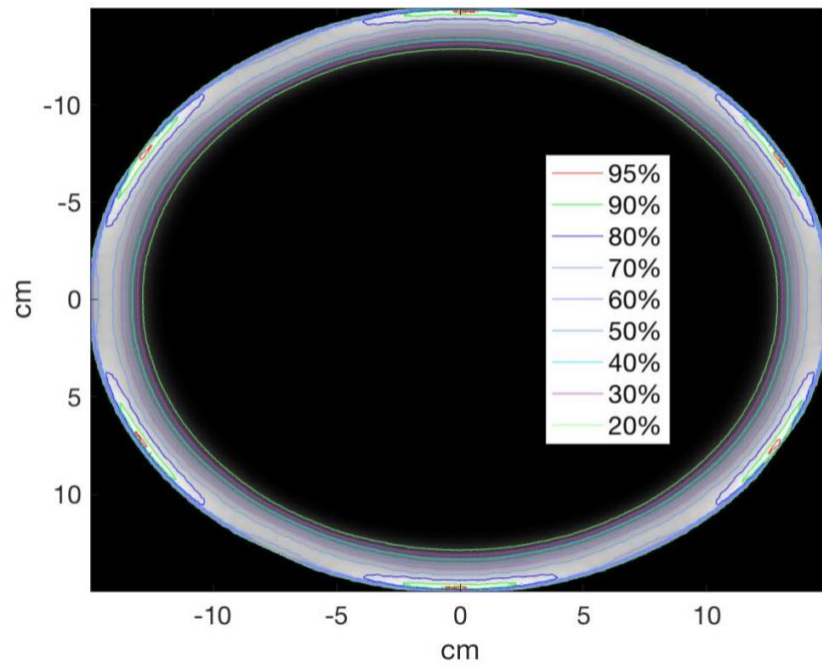


Figure 18 : Dose distribution for six dual-field electron beams at central slice

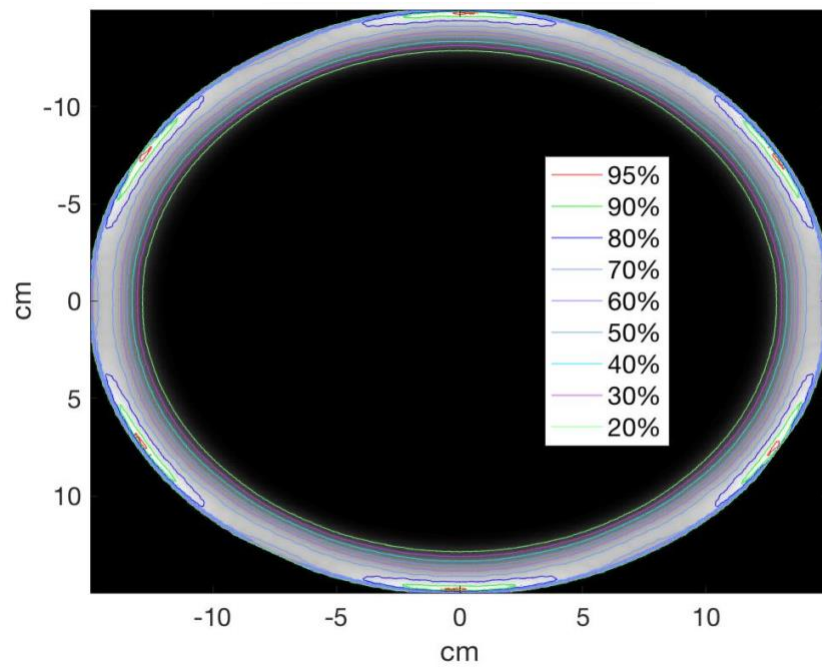


Figure 19 : Dose distribution for six dual-field electron beams at off 40 cm from the central slice

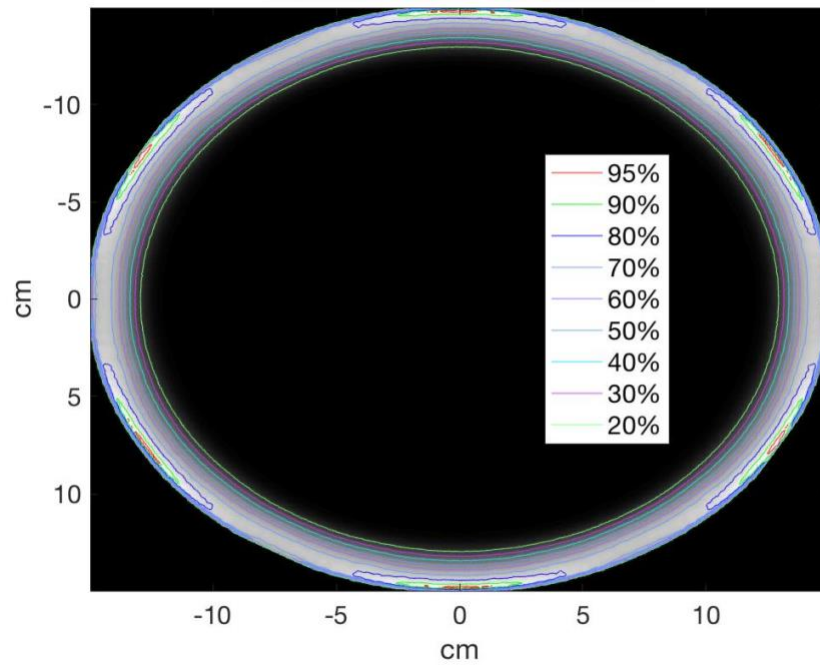


Figure 20 : Dose distribution for six dual-field electron beams at off 80 cm from the central slice

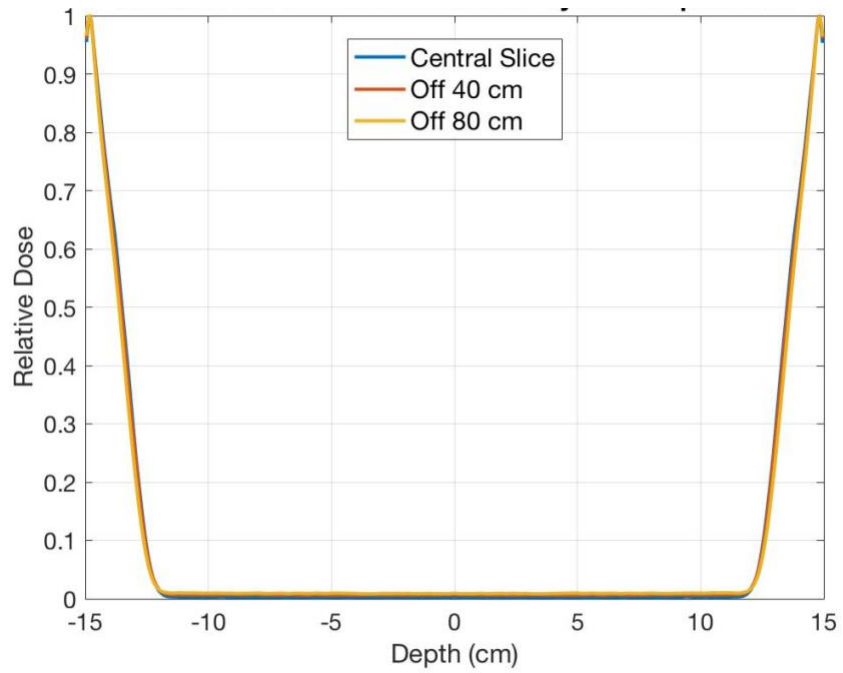


Figure 21 : Off axis PDDs (0, 40, 80 cm off the central slice) on a 30 cm diameter cylindrical phantom

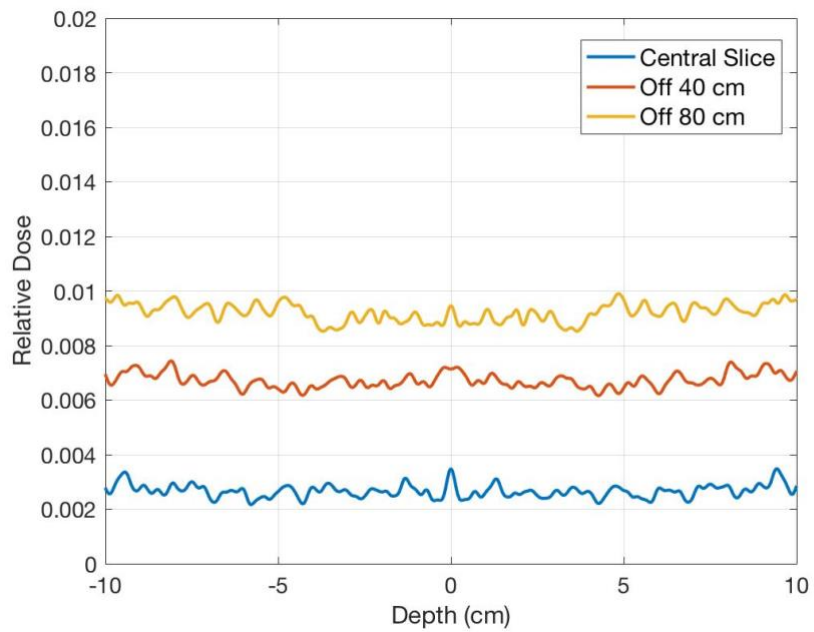


Figure 22 : The area of -10 cm to 10 cm from figure 21

3.2.3.4 Composite PDD for six dual-field electron beams on a cylindrical phantom with different sizes (20, 30, and 40 cm diameter)

Figure 23, 24, and 25 show the composite dose distribution on a 20, 30, and 40 cm diameter cylindrical phantoms respectively. This aimed to evaluate the dosimetric effect on different patient sizes (such as slender and fat patients) and size of different body regions of a patient such as the thickness of the neck is thinner, compared with the thickness of the abdomen. 30 cm diameter cylindrical phantom was assumed to be the standard patient size, while 20 cm and 40 cm diameter phantoms were simulated to be a thinner and thicker patient respectively. Table 7 lists the surface dose, B factor, and maximum x-ray contamination for these three different phantom sizes, they generally showed a similar surface dose, B-factor, and x-ray contamination, but the B-factor and x-ray contamination tend to slightly decrease when the phantom size increases.

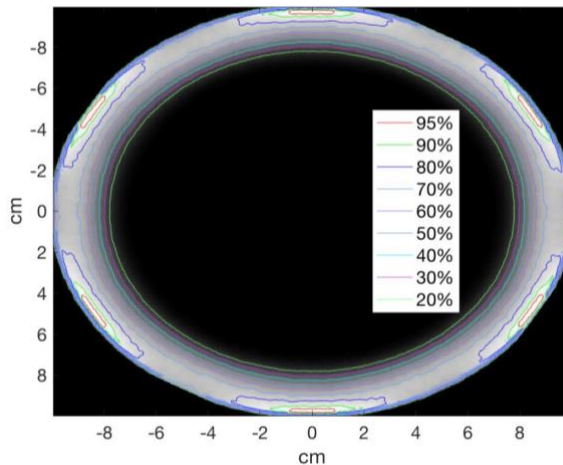


Figure 23 : Dose distribution for six dual-field electron beams on a 20 cm diameter cylindrical phantom

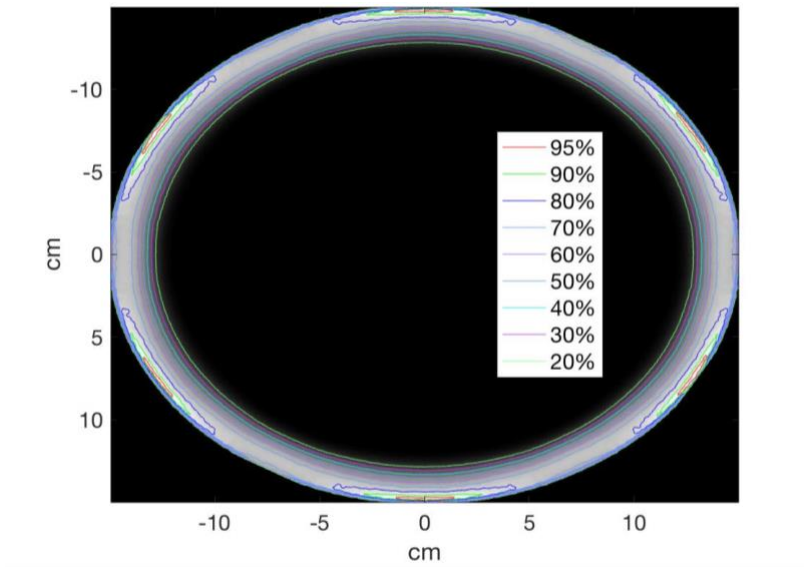


Figure 24 : Dose distribution for six dual-field electron beams on a 30 cm diameter cylindrical phantom

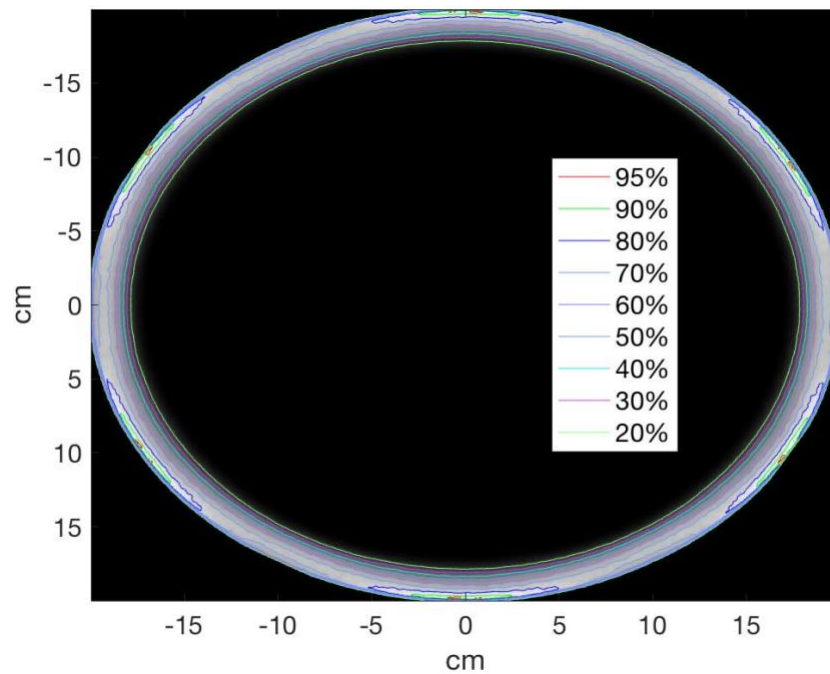


Figure 25 : Dose distribution for six dual-field electron beams on a 40 cm diameter cylindrical phantom

Table 7 : Dosimetric quantities for different phantom sizes (20, 30, and 40 cm)

Diameter (cm)	20	30	40
Surface dose (%)	96	100	94
B-factor	3.2	3.1	3.0
x-ray contamination (%)	1.4	1.3	1.0

3.2.4 Output factor, Body factor, and X-ray contamination

Output factors at the depth of the surface of one dual-field electron beam for EGSnrc and VirtuaLinac were 0.0707 and 0.0701 respectively, compared with 0.07242 in the measured data. That is, - 2.4 % and -3.2 % off the measured data for EGSnrc and VirtuaLinac respectively. The output at the depth of surface for six dual-field electron beams can be calculated by multiplying the calibration output for dual electron field and the final body factor. Body factors were 3.11 and 3.12 for EGSnrc and VirtuaLinac respectively with the measured data of 3.08. The difference was -1.1 % in EGSnrc and - 1.4 % in VirtuaLinac off the measured data. The maximum x-ray contamination for six dual-field electron beams were 1.2 % of D_{max} in EGSnrc and 1.3 % of D_{max} in VirtuaLinac, compared with less than 2 % of D_{max} in the measured data.

3.3 Validation of Monte Carlo Simulation for the Lay-down technique

3.3.1 Profiles for Vertex fields

The average difference of X profiles was 1.6 % (with maximum 3.3 % difference) in the field of 0 degrees gantry angle, while the average difference was 1.8 % (with the maximum 8.3 % difference) in the rotated fields (the gantry angle of 60 and 300 degrees), compared with the measured data, as shown in Figure 26. The maximum differences of rotated fields were located at edges (from -90 to -70 cm and 70 to 90 cm). As mentioned in the previous section 3.2, this difference may be caused by the wrong rotation of gantry angle within BEAMnrc. This problem is currently being investigated.

Although EGSnrc demonstrated a huge difference at the edges for the rotated fields, it matched well with the measured data in the Y profile (shown in Figure 27) with less than 1.2 % difference. The maximum difference in Y profile for the field of 0 degrees gantry angle was 4.9 % which was acceptable. That is, EGSnrc showed a good agreement with the measured data in Y profile.

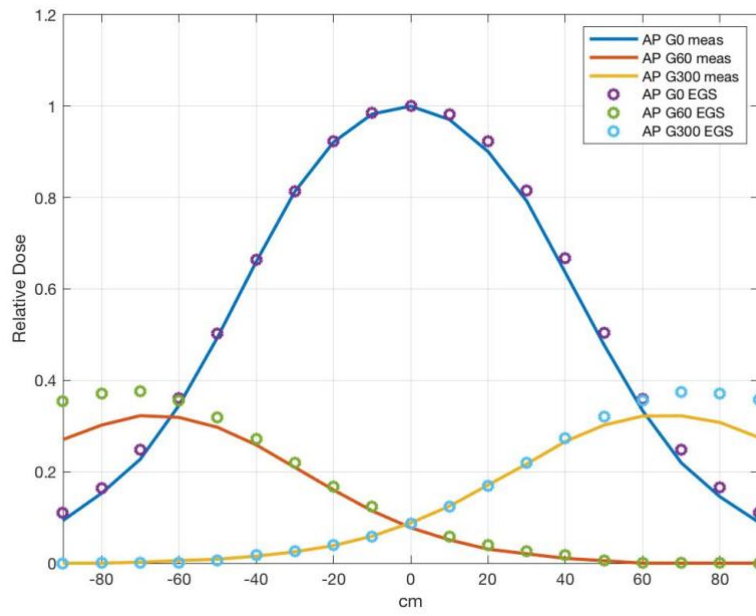


Figure 26 : X profile (1 cm depth) for Vertex fields

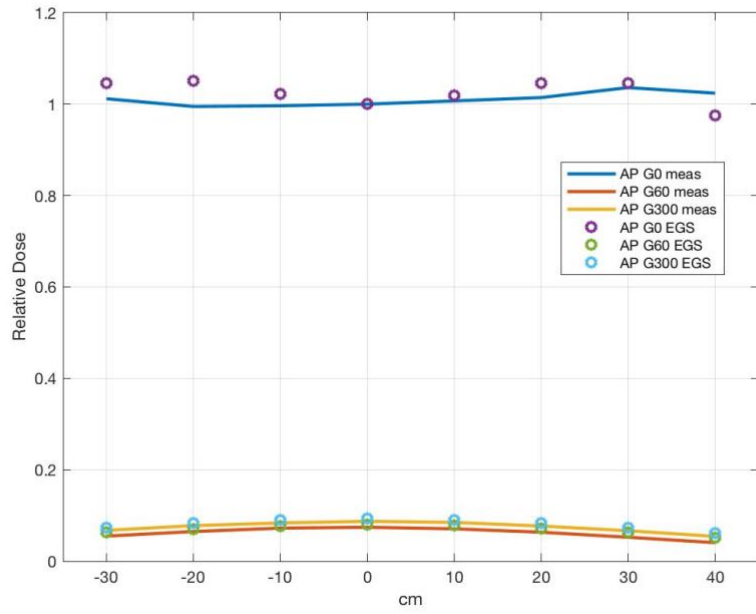


Figure 27 : Y profile (1 cm depth) for Vertex fields

3.3.2 Profiles for Oblique fields

Figure 28 shows the X profile for the oblique field in a TSI lay-down technique. The difference was within 5 % from -80 cm to 80 cm of the profile, compared with the measured data. The maximum difference was 8 % at the edges (90 and -90 cm). Again, although EGSnrc demonstrated a huge difference at the edges in the X profile, it matched well with the measured data in Y profile (shown in Figure 29) with less than 1.5 % difference.

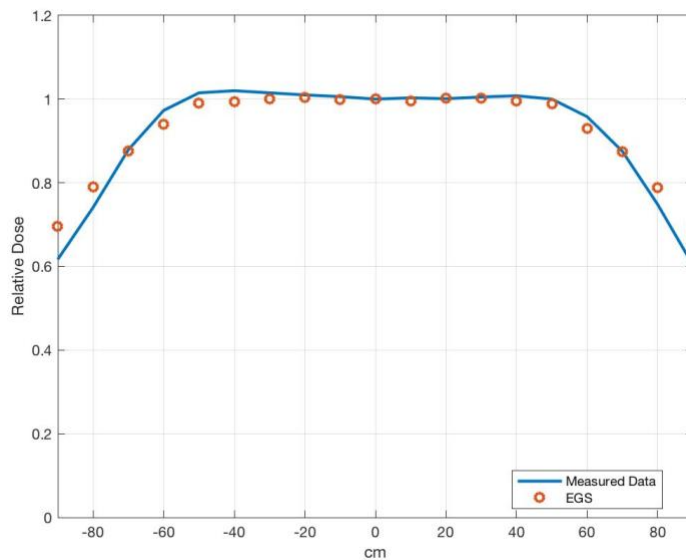


Figure 28 : X profile (1 cm depth) for Oblique field

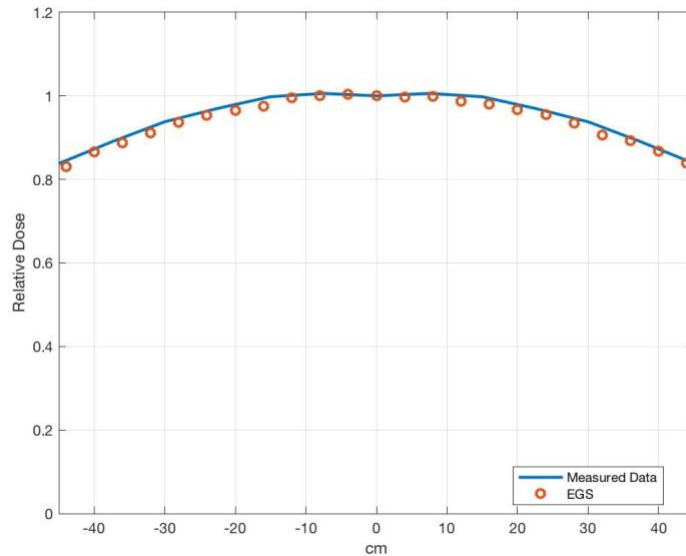


Figure 29 : Y profile (1 cm depth) for Oblique field

3.3.3 Composite dose distribution on a cylindrical phantom for the lay-down technique

Figure 30 shows the dose distribution for the composite fields on a cylindrical phantom and Figure 31 shows the PDD for 0, 30, 60 degrees of profile to evaluate the dose distribution of hot and cold areas on a cylindrical phantom. The composite dose distribution had the surface dose at 96 %, d_{max} at 0.15 cm, and R_{80} at 0.55 cm, compared with the measured value of 95.2 %, 0.15 cm, and 0.75 cm. The d_{max} shifted toward the surface of the cylindrical phantom when all fields were combined.

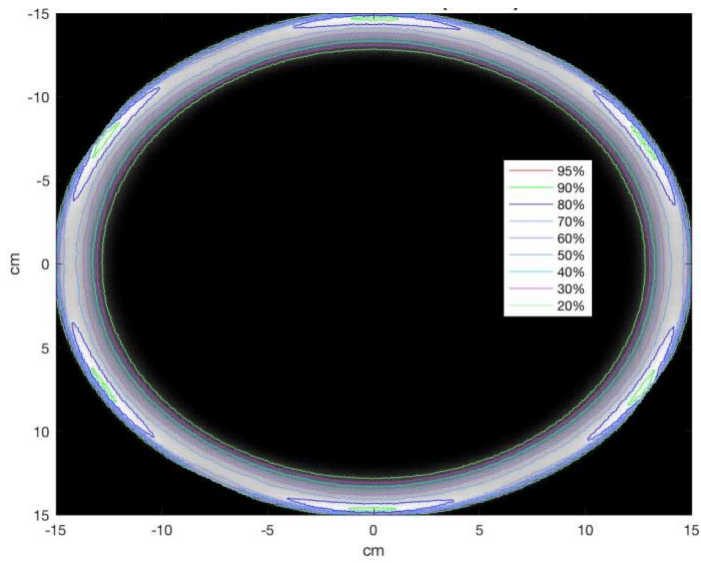


Figure 30 : Dose distribution for combination of all fields on a cylindrical phantom

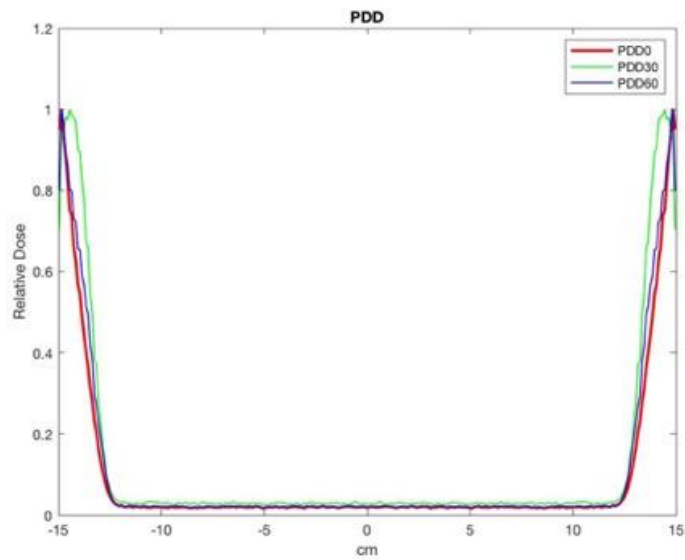


Figure 31 : PDD for 0, 30, and 60 degrees of profiles on a cylindrical phantom

3.3.4 Output factor, Body factor, and X-ray contamination

The relative output factors in the TSI laydown technique were 0.498, 0.1, 0.08, and 0.034 for isocenter, AP_G0 (AP field with gantry 0 degree), AP_G60, and OB (oblique field) respectively, compared 0.49, 0.098, 0.09, 0.034 in the measured data. The output factors from EGSnrc had a good agreement (less than 1.65 % difference) with the measured data, except the output factor for a rotated field (AP_G60), which had 4.7% difference from the measured data. Body factors for AP and LAO fields were 3.51 and 3.54, compared with 3.45 and 3.54 in the measured data. X-ray contamination were 2.2 % and 2.07 % for EGSnrc and the measured data respectively. That is, EGSnrc demonstrated a general agreement with measurement for output factors, body factors, and x-ray contamination. The dosimetric effect of different sizes (20, 30, and 40 cm diameters) of phantom were studied. The surface dose increases when the phantom size increases, while the B-factor and x-ray contamination decrease when the phantom size increases.

3.4 Investigation of effect of filter design for the stand-up technique

3.4.1 Profiles for single beam on a flat solid water phantom

Figure 32 shows the X profile of single electron beam from 300 to 550 cm SSD and the dual-field electron beam that has been used in the clinic. As can be seen, even the single beam with 550 cm SSD (maybe no treatment room can be larger than this size) still cannot reach the profile flatness as the dual-field electron beam. Therefore, a scattering filter has to be used to broaden the electron beam if we want to use a single electron beam in the TSI stand-up technique.

No material shows acceptable profile flatness ($\pm 10\%$ within the central 160 cm) at 250 cm SSD. At 300 cm SSD, Au (0.1 mm), Ag (0.25 mm), and Cu (0.45 mm) are acceptable. Zn (0.45 mm) requires 325 cm SSD to meet the requirement. Profiles for these four configurations are shown in Figure 33 and 34. In X profile, these four configurations have a similar trend and provide the acceptable flatness as a dual-field electron beam. In Y profile, these four configurations show better profile flatness than a dual-field electron beam.

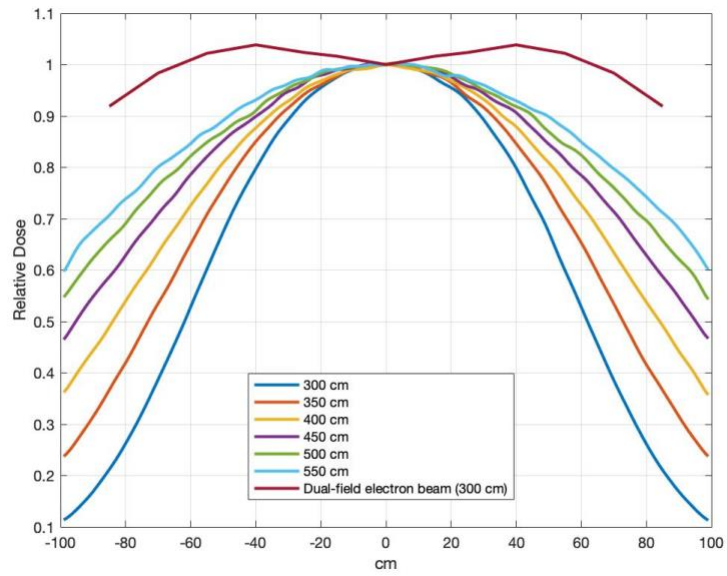


Figure 32 : X profile for single electron beam from 300 to 550 cm SSD and dual-field electron beam

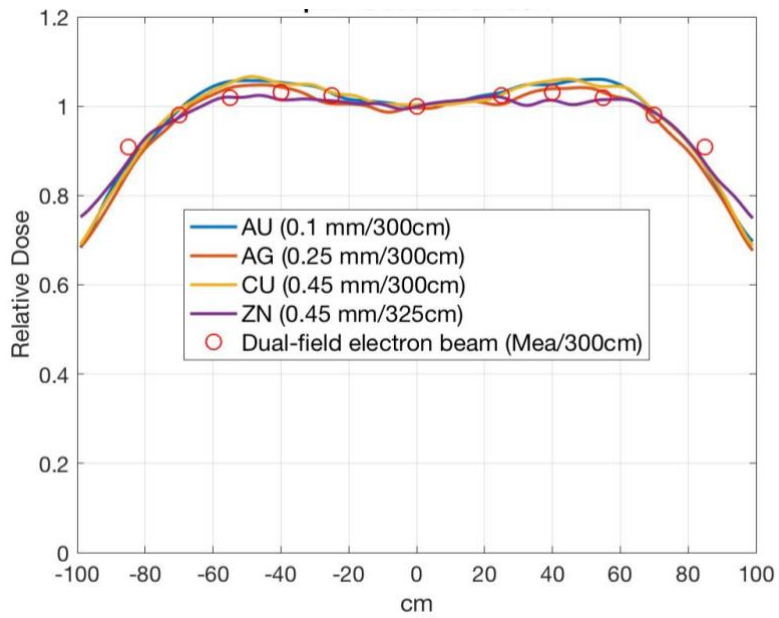


Figure 33 : X profile (1 cm depth) for these four configurations

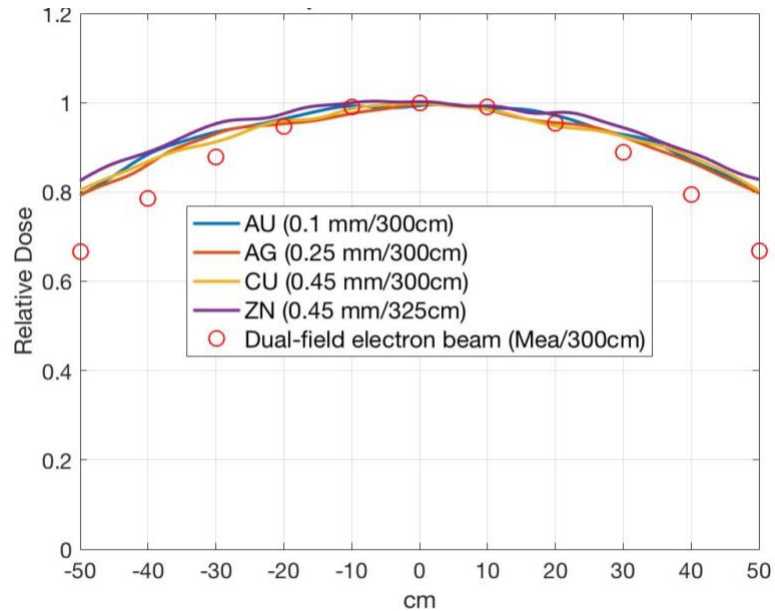


Figure 34 : Y profile (1 cm depth) for these four configurations

Figure 35 shows the PDD curve for four filter configuration, dual-field electron beam, and a single open beam at 550 cm SSD. For these four configurations, the d_{max} is 0.92-0.99 cm, similar to a dual beam (1.00 cm); R_{50} is 1.85-1.91 cm, compared with dual beam of 2.10 cm; the output factor is 0.03, lower than the dual beam (0.08). The PDD of the single electron open beam with 550 cm SSD was also plotted and compared the x-ray contamination with the four configurations (the open beam versus filtered beam). Table 8 listed the detailed dosimetric quantities of PDD at the central axis for the four filter designs, dual-field electron beam, and single beam at 550 cm SSD.

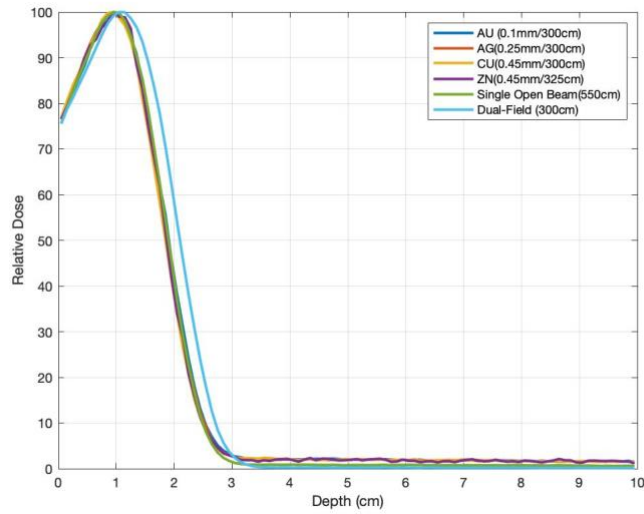


Figure 35 : PDD for four filter configurations, dual-field electron beam, and single beam (550 cm SSD)

Table 8: Dosimetric quantities for a single direction

	Dual-field	Au (0.1 mm)	Ag (0.25 mm)	Cu (0.45 mm)	Zn (0.45 mm)	Single Open
SSD (cm)	300	300	300	300	325	550
Average d_{max}	0.97	0.94	0.95	0.92	0.98	0.95
R_{50}	2.06	1.91	1.89	1.85	1.87	1.90
X-ray contamination (%)	0.2	1.71	1.72	1.75	1.73	0.86
Output Factor	0.08	0.03	0.03	0.03	0.03	0.03
# MC to get 150 cGy	1875	5000	5000	5000	5000	5000

3.4.2 Dose distribution for composite fields on a cylindrical phantom

Figure 36 shows the composite PDD for these four filter designs. The composite fields for these filter designs, the d_{\max} is 0.1 cm, compared with a dual beam (0.16 cm). The surface dose is 98-99 %, similar to a dual beam (97 %). B-factor is 3.4, compared with a dual beam (3.1). The maximum x-ray contamination is 3 %, slightly higher than a dual beam (2 %). The detailed dosimetric quantities were listed in Table 9.

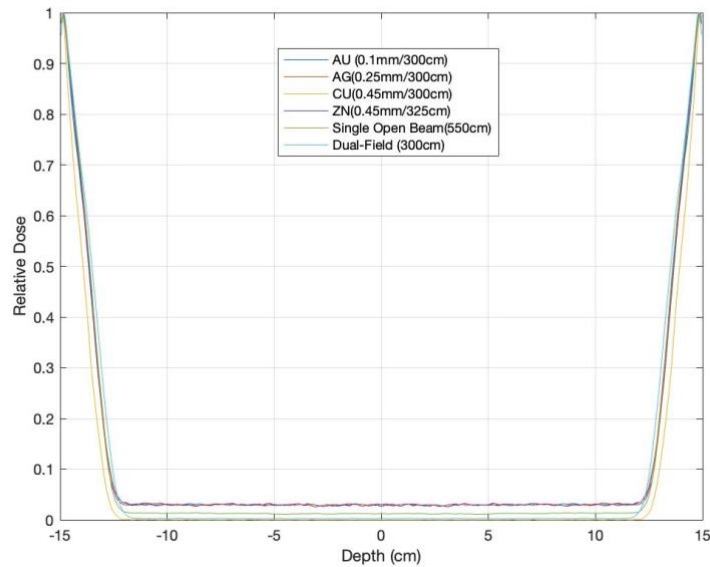


Figure 36 : Composite PDD for four filter configuration, six dual-field electron beam, and single open beam at 550 cm SSD.

Table 9: Dosimetric quantities for composite fields

	Dual-field (300 cm)	Au (0.1 mm)	Ag (0.25 mm)	Cu (0.45 mm)	Zn (0.45 mm)	Single Open (550 cm)
Average d_{\max} (mm)	1.6	1.0	1.0	1.0	1.0	1.0
Surface dose (%)	97.0	98.6	98.7	98.8	98.8	98.5
B-factor	3.1	3.4	3.4	3.4	3.4	3.4
X-ray contamination (%)	2.0	3.1	2.9	3.2	3.1	2.9

For these four filter designs, the surface dose along superior to inferior direction ranges from 97.5 % to 99.5 % (shown in Figure 37), the average dose is 98.6%, 98.7%, 98.8 %, and 98.8 % for Au, Ag, Cu, and Zn respectively. The x-ray contamination along superior to inferior direction is 0 % to 3 % (shown in Figure 38), while the average x-ray contamination is 1.2 %, 1.2 %, 1.1 %, and 1.2 % for Au, Ag, Cu, and Zn respectively.

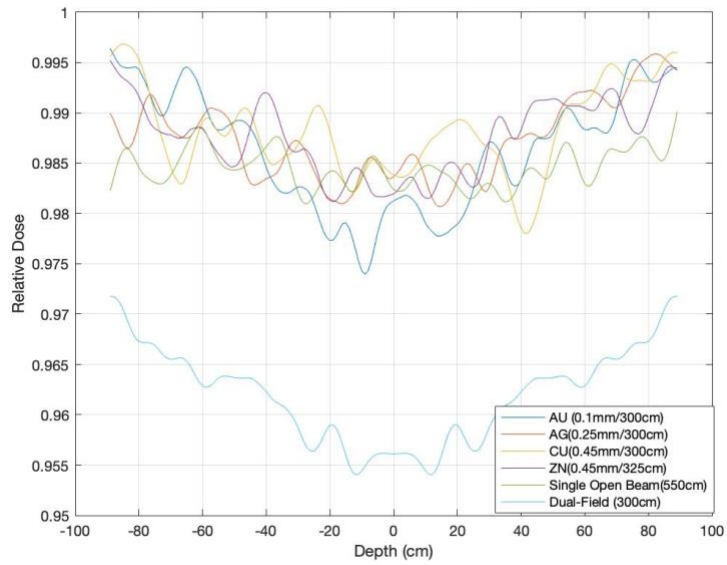


Figure 37 : Surface dose from superior to inferior direction

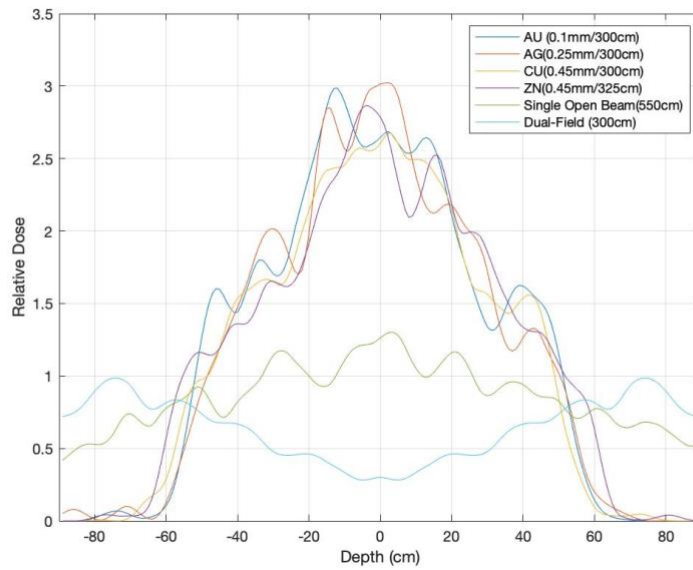


Figure 38 : X-ray contamination from superior to inferior direction

4. Future Work

4.1 Investigation of the gantry rotation issue in EGSnrc

In the EGSnrc environment, when the gantry is rotated to simulate the angled fields in TSI techniques, profiles of the angled fields always show more than 5 % maximum differences, compared to the available measured data. This difference will result in a different dose distribution on a cylindrical phantom when all the treatment fields are combined together in both TSI stand-up and lay-down techniques. This problem may be caused by a wrong rotation coordinate used within BEAMnrc and the phase-space files are not correctly rotated.

In order to investigate this rotation problem, the main phase-space file (a huge one) used in this study should be fully analyzed and compared with the original phase-space files provided by the vendor. Furthermore, the angled fields in VirtuaLinac performed well and agreed with the measured data within an acceptable tolerance, so it can be used to verify the results from EGSnrc and evaluate the factors that should be further investigated. Instead of rotating the phase-space file, another way can be used to simulate the rotated fields is to rotate the phantom in the MC simulations. In this way, we can evaluate if the phase-space files were correctly rotated in the MC simulations

4.2 Implementation of a customized scattering filter within VirtuaLinac

VirtuaLinac is a useful MC tool and it shows a good agreement with the measured data for the TSI stand-up technique. However, in the TSI lay-down technique, the results from the VirtuaLinac with a scattering filter didn't perform well and had a huge difference from the measured data, which might be caused by the inaccurate geometry or material of the scattering filter in VirtuaLinac. That is the reason why VirtuaLinac didn't be used to validate the TSI lay-down technique. In the future, a customized copper filter could be mounted with the accurate material and geometry in VirtuaLinac by the help of Varian's engineers. If this scattering filter can be successfully mounted in VirtuaLinac, it can not only be used to validate the TSI lay-down technique, but also be a reference to investigate the current rotated problems mentioned in section 4.1.

4.3 Optimization for the current standard TSI stand-up technique

A previous study [8][9] had used the custom-built scatter filter constructed of Al, Pb, and PMMA to broaden and scatter the electron beam. In our study, high atomic number materials such as Au, Ag, Zn, Fe, and Cu were chosen because of their stability and availability. The four configurations, Au (0.1 mm/300 cm), Ag (0.25 mm/300 cm), Cu (0.45 mm/300 cm) and Zn (0.45 mm/325 cm), showed the acceptable profile flatness (± 10

% over central 160 cm region) as the dual-field electron beam that has been used in the clinic.

However, for the single electron beam, the x-ray contamination at the depth of 15 cm on the 30 cm diameter cylindrical phantom is always higher than the dual-field electron beam. The maximum x-ray contamination of these four filter designs is 3 %, compared with less than 2 % in the measured data. This relatively higher x-ray contamination for a single beam may result in higher dose being delivered to all the patient body. Therefore, this higher x-ray contamination should be further studied to evaluate if a single beam could be appropriately used to treat patients.

5. Conclusion

Both TSI stand-up and lay-down techniques were implemented and commissioned at our clinic. The MC results from EGSnrc and VirtuaLinac for TSI stand-up technique in general agree well with the dosimetric data during TSI commissioning, providing the evidence that Monte Carlo can be a promising tool in dosimetry calculations for future studies. In addition to those measurable quantities such d_{\max} , R_{50} , profiles, and output factor, the Monte Carlo systems can provide further information such as full dose distribution of the patient phantom, thus Monte Carlo systems can become the foundation and guidance for investigations in future technique optimizations. The results of this research study also demonstrated that Monte Carlo methods can complement experimental hand-on measurements needed during the commissioning for new techniques. In this way, the efficiency of commissioning a new technique can be improved using the Monte Carlo methods.

Regarding the single electron beam for the standard stand-up TSI technique, the result from EGSnrc suggests the stand-up technique can be implemented using a single beam if the customized filter is used. That is, a single beam can provide an equivalent dose uniformity as the dual-field electron beam with the customized filter is mounted. However, the relatively higher x-ray contamination shown in the MC simulations on the cylindrical phantom and the fluctuated x-ray contamination along superior to inferior direction should be further investigated to evaluate if a single beam could be used to

treat a real patient. To obtain a more precise dose distribution in a real patient, CT-based anthropomorphic phantom can be used to calculate the x-ray contaminations at different locations by inserting EBT3 films and placing OLSDs in the phantom for the future study. Furthermore, the actual manufacturing and measurement have to be performed to validate these simulations results.

References

- [1] Karzmark CJ, Anderson J, Buffa A et al. *Total skin electron therapy: technique and dosimetry*. AAPM Report 23. Task Group 30 Radiation Committee. New York: American Institute of Physics; 1987.
- [2] Wu JM, Leung SW, Wang CJ, Chui CS. *Lying-on position of total skin electron therapy*. Int J Radiat Oncol Biol Phys. 1997;39(2):521–2
- [3] Deufel, Christopher L and John A Antolak. *Total skin electron therapy in the lying-on-the-floor position using a customized flattening filter to eliminate field junctions*. Journal of applied clinical medical physics vol. 14,5 115-26. 6 Sep. 2013
- [4] Nevelsky A, Borzov E, Daniel S, Bar-Deroma R et al. *Validation of total skin electron irradiation (TSEI) technique dosimetry data by Monte Carlo simulation*. Journal of Applied Clinical Medical Physics; 2016
- [5] Nevelsky A, Borzov E, Daniel S, Bar-Deroma R et al. *Room scatter effects in Total Skin electron Irradiation: Monte Carlo simulation study*. Journal of Applied Clinical Medical Physics; 2017
- [6] Ester Carrasco Pavon et al. *Total skin electron therapy treatment verification: Monte Carlo simulation and beam characteristics of large non-standard electron fields*. Phy. Med. Biol. 48 2783; 2003
- [7] Ye, Sung-Joon & Pareek, Prem & Spencer, Sharon & Duan, Jinxiu & Brezovich, Ivan. *Monte Carlo techniques for scattering foil design and dosimetry in total skin electron irradiations*. Medical physics. 32. 1460-8. 10.1118/1.1924368; 2005
- [8] Reynard, Eric P et al. "Rotational total skin electron irradiation with a linear accelerator" *Journal of applied clinical medical physics* vol. 9,4 2793. 3 Nov. 2008, doi:10.1120/jacmp.v9i4.2793
- [9] Evans, Michael D C et al. "Institutional experience with a rotational total skin electron irradiation (RTSEI) technique-A three decade review (1981-2012)" *Reports of practical oncology and radiotherapy : journal of Great Poland Cancer Center in Poznan and Polish Society of Radiation Oncology* vol. 19,2 120-34. 17 Jun. 2013, doi:10.1016/j.rpor.2013.05.002
- [10] Ruiqi Li, *Validation of dosimetry for a lay-down Total Skin Irradiation Techniques by Monte Carlo Simulation*, master thesis, Duke University, 2019